Article

Neuron

Tmem100 Is a Regulator of TRPA1-TRPV1 Complex and Contributes to Persistent Pain

Highlights

- A unique context-dependent TRP channel regulation by disinhibitory mechanism
- Tmem100 as a potentiating modulator of TRPA1 in the TRPA1-TRPV1 complex
- Tmem100-mutant-derived cell-permeable peptide as novel pain therapeutics
- The first mechanistic study of *Tmem100*, an important gene implicated in diseases

Authors

Hao-Jui Weng, Kush N. Patel, ..., Armen N. Akopian, Xinzhong Dong

Correspondence

akopian@uthscsa.edu (A.N.A.), xdong2@jhmi.edu (X.D.)

In Brief

TRPA1 and TRPV1 are crucial pain mediators, but how their interaction contributes to persistent pain is unknown. Weng et al. identify Tmem100 as a potentiating modulator of TRPA1-V1 complexes. Targeting this modulation, they developed a strategy for blocking persistent pain.

Weng et al., 2015, Neuron *85*, 833–846
February 18, 2015
http://dx.doi.org/10.1016/j.neuron.2014.12.065

CellPress

Neuron
Article

Tmem100 Is a Regulator of TRPA1-TRPV1 Complex and Contributes to Persistent Pain

Hao-Jui Weng,[1,2] Kush N. Patel,[1] Nathaniel A. Jeske,[3] Sonya M. Bierbower,[3] Wangyuan Zou,[4] Vinod Tiwari,[5] Qin Zheng,[1] Zongxiang Tang,[6] Gary C.H. Mo,[7] Yan Wang,[1,8] Yixun Geng,[1] Jin Zhang,[1,7] Yun Guan,[5] Armen N. Akopian,[9,*] and Xinzhong Dong[1,10,*]

[1]Departments of Neuroscience and Neurosurgery, School of Medicine, Johns Hopkins University, Baltimore, MD 21205, USA
[2]Department of Dermatology, National Taiwan University Hospital, Taipei City 100, Taiwan
[3]Department of Physiology, University of Texas Health Science Center, San Antonio, TX 78229, USA
[4]Department of Anesthesiology, Xiangya Hospital, Central South University, Changsha, Hunan 410008, China
[5]Department of Anesthesiology and Critical Care, School of Medicine, Johns Hopkins University, Baltimore, MD 21205, USA
[6]Nanjing University of Chinese Medicine, Nanjing 210046, China
[7]Department of Pharmacology and Molecular Sciences, School of Medicine, Johns Hopkins University, Baltimore, MD 21205, USA
[8]West China School of Stomatology, Sichuan University, Chengdu, Sichuan 610041, China
[9]Department of Endodontics, University of Texas Health Science Center, San Antonio, TX 78229, USA
[10]Howard Hughes Medical Institute, Johns Hopkins University School of Medicine, Baltimore, MD 21205, USA
*Correspondence: akopian@uthscsa.edu (A.N.A.), xdong2@jhmi.edu (X.D.)
http://dx.doi.org/10.1016/j.neuron.2014.12.065

SUMMARY

TRPA1 and TRPV1 are crucial pain mediators, but how their interaction contributes to persistent pain is unknown. Here, we identify Tmem100 as a potentiating modulator of TRPA1-V1 complexes. Tmem100 is coexpressed and forms a complex with TRPA1 and TRPV1 in DRG neurons. Tmem100-deficient mice show a reduction in inflammatory mechanical hyperalgesia and TRPA1- but not TRPV1-mediated pain. Single-channel recording in a heterologous system reveals that Tmem100 selectively potentiates TRPA1 activity in a TRPV1-dependent manner. Mechanistically, Tmem100 weakens the association of TRPA1 and TRPV1, thereby releasing the inhibition of TRPA1 by TRPV1. A Tmem100 mutant, Tmem100-3Q, exerts the opposite effect; i.e., it enhances the association of TRPA1 and TRPV1 and strongly inhibits TRPA1. Strikingly, a cell-permeable peptide (CPP) containing the C-terminal sequence of Tmem100-3Q mimics its effect and inhibits persistent pain. Our study unveils a context-dependent modulation of the TRPA1-V1 complex, and Tmem100-3Q CPP is a promising pain therapy.

INTRODUCTION

Pain is the cardinal symptom of many debilitating diseases, causing heavy societal and health burdens worldwide. It is known that ion channels and receptors in the dorsal root ganglia (DRG) are responsible for the detection of noxious stimuli, and their plasticity contributes to the increased severity of pain (Woolf and Costigan, 1999). TRP (*t*ransient *r*eceptor *p*otential) channels are emerging targets for understanding this process and developing novel treatments (Venkatachalam and Montell, 2007). Their ability to form multimeric complexes (Goel et al., 2002; Hellwig et al., 2005; Hofmann et al., 2002; Schaefer, 2005; Strübing et al., 2001; Xu et al., 1997) broadens the variety and complexity of channel regulation and the potential implications for pain modulation (Jeske et al., 2011; Liu et al., 2011; Patil et al., 2011; Schmidt et al., 2009). Among TRP channels, TRPA1 and TRPV1 are essential and widely studied molecular sensors and mediators of pain signals in DRG neurons (Bautista et al., 2006; Caterina et al., 2000; Caterina et al., 1997). It is well documented that most if not all TRPA1$^+$ DRG neurons coexpress TRPV1 (Bautista et al., 2006; Story et al., 2003). Although recent studies have suggested that TRPA1 and TRPV1 can form a complex in a heterologous expression system as well as sensory neurons (Fischer et al., 2014; McMahon and Wood, 2006; Salas et al., 2009; Staruschenko et al., 2010), the functional significance and modulation of the complex in the nociceptive pathway are unclear.

We identified Tmem100 as a candidate for the modulation of the TRPA1-V1 complex in the nociceptive pathway. Tmem100 is a 134-amino-acid, two-transmembrane protein highly conserved in vertebrates (Moon et al., 2010). It is found in other organs besides the DRG, expressed in blood vessels, ventral neural tubes, and the notochord (Moon et al., 2010). Tmem100 has been shown to be involved in processes such as renal development (Georgas et al., 2009), vasculogenesis (Moon et al., 2010), and lung cancer cell invasiveness (Frullanti et al., 2012). However, little is known about the underlying mechanisms of these effects and the role of Tmem100 in the nervous system.

Here, we demonstrate that Tmem100 enhances TRPA1 activity in vitro and in vivo. Interestingly, this regulation depends on the presence of TRPV1. In the DRG, Tmem100 is coexpressed with TRPA1 and TRPV1. It forms a complex with TRPA1 and TRPV1 in both DRG neurons and heterologous systems. Tmem100 selectively augments TRPA1-associated activity by increasing the open probability of the channel when TRPA1 and TRPV1 are both present in membrane patches. Tmem100 mutant mice exhibit a reduction in inflammatory mechanical

hyperalgesia and TRPA1- but not TRPV1-mediated pain. Mechanistically, Tmem100 weakens the association of TRPA1 and TRPV1, thereby releasing the inhibition of TRPA1 by TRPV1 (Salas et al., 2009). A Tmem100 mutant, Tmem100-3Q, exerts the opposite effect; i.e., it enhances the association of TRPA1 and TRPV1 and strongly inhibits TRPA1. Taking advantage of this inhibition, we developed a new strategy for blocking persistent pain. We designed a cell-permeable peptide that mimics the C terminus of Tmem100-3Q and selectively inhibits TRPA1-mediated activity and pain in a TRPV1-dependent manner.

RESULTS

Tmem100 Encodes a Two-Transmembrane Protein Expressed in Peptidergic DRG Neurons

We investigated the topology of Tmem100 to understand its cellular localization and distribution. Protein structure analysis (PredictProtein, Columbia University, and SOSUI, Nagoya University, Japan) indicates that Tmem100 is a two-transmembrane protein (Figure 1A). We transfected a *Tmem100-myc* construct with c-*myc* at the C terminus into the F11 cell line and stained with anti-myc antibody. Tmem100 was visualized at the plasma membrane only after membrane permeabilization (Figures S1A and S1C available online). Similar results were obtained with anti-Tmem100 antibody against the N terminus (Figure S1B). Staining also showed that the signal was primarily located in the plasma membrane (Figure S1D). The data indicate that Tmem100 is a two-transmembrane protein largely localized to the plasma membrane with intracellular localization of both N and C termini.

To characterize *Tmem100*-expressing DRG neurons, we generated a knockin line in which the open reading frame of *Tmem100* was replaced with GFP ($Tmem100^{GFP/+}$; Figures S1E and S1F). Anti-Tmem100 antibody labeling confirmed that GFP is specifically expressed in $Tmem100^{+}$ DRG neurons in the $Tmem100^{GFP/+}$ mouse line (Figure S1F). Using GFP as a marker, we found that *Tmem100* was expressed in 24% of lumbar DRG neurons (mainly small and medium in size) (Figure 1B). We double stained different DRG neuron markers with GFP in the $Tmem100^{GFP/+}$ line (Figures 1C, 1D, and S1G). Ninety-five percent of $Tmem100^{+}$ neurons express CGRP, and 88.4% of $CGRP^{+}$ neurons express Tmem100. Both TRPA1 and TRPV1 are coexpressed in a subset of $Tmem100^{+}$ neurons. In contrast, $Tmem100^{+}$ neurons were rarely positive for IB_4 (Figures 1C, 1D, and S1). These results suggest that *Tmem100* is primarily expressed in peptidergic DRG neurons (Figure 1E), many of which are TRPV1 and TRPA1 double positive (Figure 1F) (Bautista et al., 2006; Story et al., 2003). A recent study has shown that TRPA1 is functionally expressed in $IB4^{+}$ nonpeptidergic neurons (Barabas et al., 2012). The culture conditions of dissociated DRG neurons can influence the expression of TRPA1. On the other hand, the sensitivity of anti-TRPA1 antibody may miss the expression of TRPA1 in $IB4^{+}$ neurons. Moreover, we found a significant increase in the number of Tmem100-expressing neurons in the DRG under inflammatory conditions induced by complete Freund's Adjuvant (CFA) injection (Figures S1H and S1I). Collectively, the expression data suggest that Tmem100 may be involved in the modulation of pain.

Selective Elimination of *Tmem100* in Sensory Neurons Leads to a Reduction of Mechanical Hyperalgesia and TRPA1-Associated Nociception

Conditional knockout mice were generated to study the function of Tmem100 in the nociceptive pathway ($Tmem100^{fl/fl}$; Figure 2A) because a global knockout of *Tmem100* is lethal at E10.5 (Moon et al., 2010). $Tmem100^{fl/fl}$ mice were mated with male $Advillin^{+/CRE}$ (Avil-Cre) mice to selectively eliminate *Tmem100* in primary sensory neurons of the DRG (Hasegawa et al., 2007). These mice were viable, and there were no obvious differences in gross appearance and behavior among wild-type (WT), *Avil-Cre;*$Tmem100^{+/+}$, $Tmem100^{fl/fl}$, and *Avil-Cre;*$Tmem100^{fl/fl}$ mice. The deletion of Tmem100 protein in the DRG was verified by immunofluorescent staining and western blotting with a rabbit anti-Tmem100 antibody (Figures 2B and S2A). We did not observe any significant changes in TRPA1 and TRPV1 expression in the DRG when Tmem100 was eliminated (Figures S2A–S2C). Moreover, developmental and morphological phenotypes were evaluated in the DRG and spinal cord from *Avil-Cre;* $Tmem100^{GFP/fl}$ lines, and the results did not suggest any related defects (Figures S2D–S2F).

We next determined whether Tmem100 plays a role in nociception and hyperalgesia/allodynia by performing behavioral tests on Tmem100 DRG conditional knockout mice, i.e., *Avil-Cre;*$Tmem100^{fl/fl}$ (*Tmem100* CKO). These mice exhibited normal mechanical sensitivity under naive conditions (Figure 2C). However, *Tmem100* CKO mice exhibited reduced acute nocifensive behaviors induced by mustard oil (MO; an agonist of TRPA1 [Bautista et al., 2006; Kwan et al., 2006]) compared to *Avil-Cre;*$Tmem100^{+/+}$ and $Tmem100^{fl/fl}$ controls (Figures 2D and S2G). TRPA1-dependent mechanical hyperalgesia generated by injection of MO into mouse hindpaws (Bautista et al., 2006) was also significantly decreased in *Tmem100* CKO mice (Figure 2E). The average threshold for mechanically induced pain was reduced to 0.06 g in both control groups and was significantly higher (0.34 g) in *Tmem100* CKO mice. In the inflammatory pain model generated by injection of CFA into the hindpaws, *Tmem100* CKO mice also showed attenuated mechanical hyperalgesia (Figure 2G), consistent with a previous report on the involvement of TRPA1 in inflammatory mechanical hyperalgesia (Petrus et al., 2007). The mechanical nociceptive threshold was reduced to 0.18 and 0.11 g in *Avil-Cre;*$Tmem100^{+/+}$ and $Tmem100^{fl/fl}$ mice, respectively, but was 0.43 g in *Tmem100* CKO mice at day 2. These data show that deletion of *Tmem100* in the DRG leads to a substantial reduction of inflammatory mechanical hyperalgesia and acute TRPA1-associated nociception.

Interestingly, TRPV1-associated acute nociceptive behavior and hyperalgesia remained relatively unperturbed in *Tmem100* CKO mice. Tmem100 CKO mice did not show any significant deficits in capsaicin-induced acute nocifensive behavior in the hindpaw (Figure 2F). Tail immersion and hot plate tests also failed to reveal any deficits in the mutant mice (Figures 2I and 2J). Furthermore, CFA-induced thermal hyperalgesia, which is almost completely reversed after TRPV1 deletion but unaltered after pharmacological blockade of TRPA1 (Caterina et al., 2000; Petrus et al., 2007), was also unchanged in *Tmem100* CKO mice (Figure 2H). We also tested cold-induced pain in these

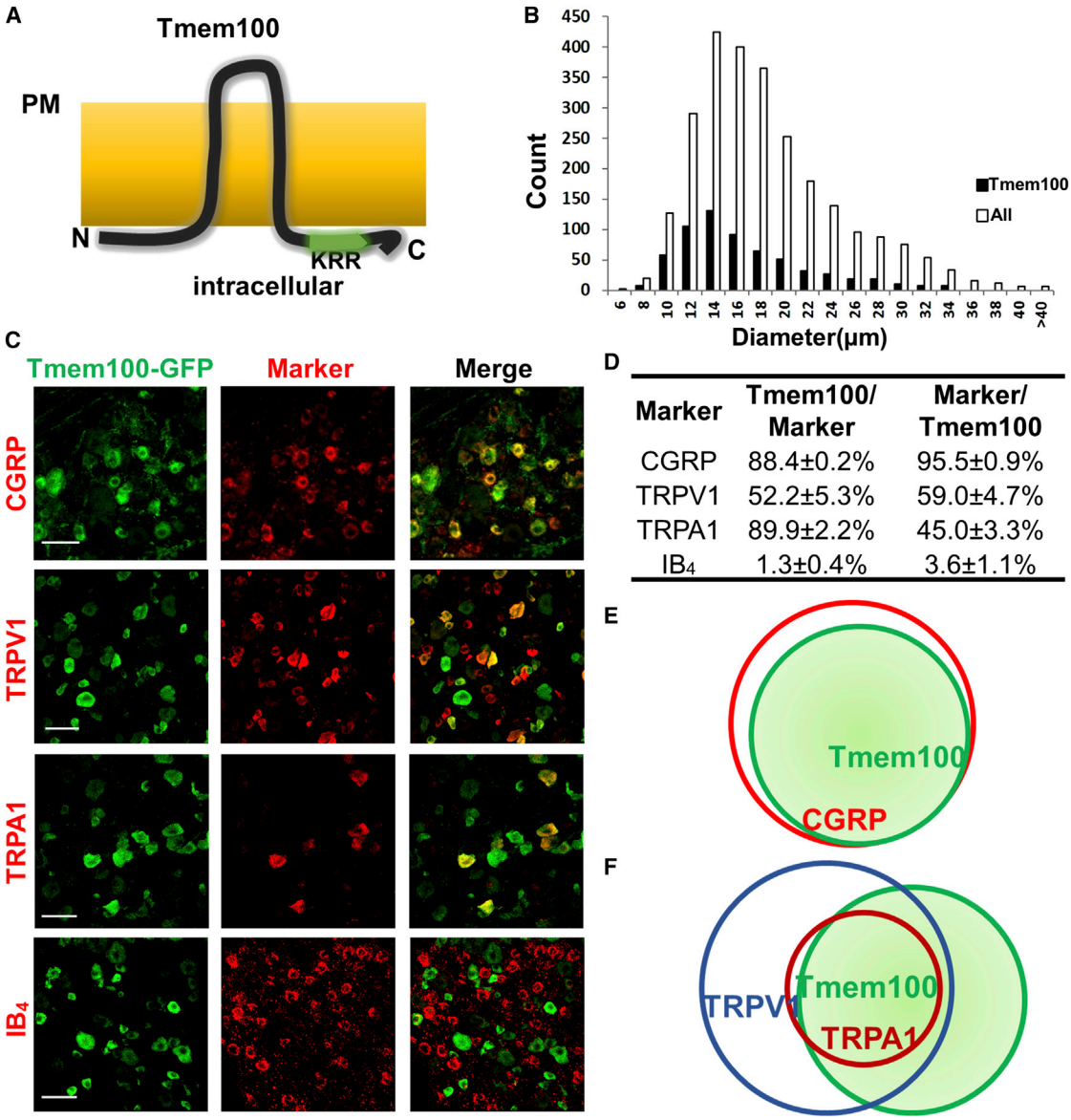

Marker	Tmem100/ Marker	Marker/ Tmem100
CGRP	88.4±0.2%	95.5±0.9%
TRPV1	52.2±5.3%	59.0±4.7%
TRPA1	89.9±2.2%	45.0±3.3%
IB_4	1.3±0.4%	3.6±1.1%

Figure 1. Tmem100 Is Expressed in TRPA1-TRPV1-Positive Peptidergic DRG Neurons

(A) Postulated structure of Tmem100. Tmem100 is a two-transmembrane protein with a putative TRPA1 binding site (KRR) at its C terminus. Both the N and C termini are intracellular, whereas the loop region is extracellular. PM, plasma membrane.

(B) *Tmem100*-expressing cells comprise 24% of L4-L6 DRG neurons. They are predominantly small-diameter, but medium- to large-diameter neurons are also present. The average diameter of *Tmem100*-expressing neurons is 15.7 μm, and the median is 14.3 μm (DRG from three mice).

(C) Double staining of Tmem100-GFP with other DRG markers. Scale bar, 50 μm.

(D) Quantification of coexpression of *Tmem100* and other DRG markers (DRG from three mice; data are presented as mean ± SEM).

(E and F) Diagrams showing the relationship of Tmem100 with other DRG markers. Tmem100 is a marker for the majority of $CGRP^+$ DRG neurons (E); most $TRPA1^+$ DRG neurons express *Tmem100* (F).

animals, and the results suggest that this modality is not affected by the elimination of Tmem100 (Figures S2H and S2I).

TRPA1-Mediated Responses Are Selectively Attenuated in DRG Neurons from *Tmem100* CKO Mice

To investigate the function of Tmem100 at a cellular level, cultured DRG neurons from *Tmem100* CKO mice were examined with calcium imaging and whole-cell electrophysiology recording. The results showed a selective reduction in TRPA1- but not TRPV1- or TRPM8-mediated activities in the DRG neurons when Tmem100 was deleted. In calcium imaging, only IB4-negative DRG neurons were analyzed because the majority of $IB4^+$ neurons do not express Tmem100 (in cultured conditions, only 4.8% ± 0.8% $IB4^+$ neurons expressed Tmem100, and 5.2% ± 0.5% of $Tmem100^+$ neurons were $IB4^+$; >900 neurons from three mice were analyzed for each marker). The

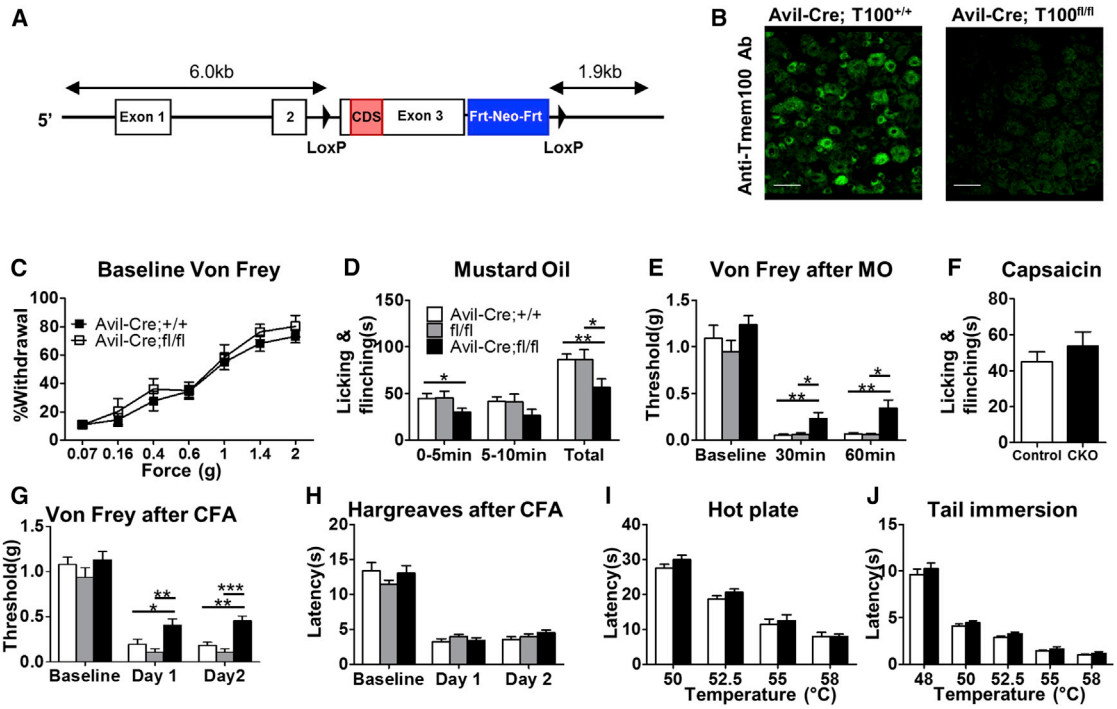

Figure 2. *Tmem100* CKO Mice Show Selective Deficits in TRPA1-Associated Behaviors, whereas TRPV1-Associated Behaviors Are Unaffected

(A) *Tmem100* conditional KO strategy.

(B) Deletion of the *Tmem100* gene in conditional KO lines was verified by anti-Tmem100 immunostaining of DRG. Scale bar, 50 μm.

(C) The baseline mechanical sensitivity of *Tmem100* CKO (*Avil-Cre;Tmem100$^{fl/fl}$*) mice is similar to that of the control group (*Avil-Cre;Tmem100$^{+/+}$* mice). At the forces tested, there was no significant difference in the response rate among *Tmem100* CKO and the control group (n = 10 for CKO and 13 for control).

(D) *Tmem100* CKO mice showed decreased acute nocifensive behavior after 0.2% MO injection. White bar, *Avil-Cre;Tmem100$^{+/+}$*; gray bar, *Tmem100$^{fl/fl}$*; black bar, *Avil-Cre;Tmem100$^{fl/fl}$*. Total time of licking and flinching: 86 ± 6.2 s in *Avil-Cre;Tmem100$^{+/+}$*; 86 ± 11.1 s in *Tmem100$^{fl/fl}$*; 57 ± 9.3 s in *Tmem100* CKO; n = 13 for *Avil-Cre;Tmem100$^{+/+}$* and *Tmem100$^{fl/fl}$* ; n = 10 for *Tmem100* CKO. *p < 0.05, **p < 0.01.

(E) *Tmem100* CKO mice showed decreased mechanical hyperalgesia after MO injection (n = 11 for *Avil-Cre;Tmem100$^{+/+}$;* 9 for *Tmem100$^{fl/fl}$* ; 10 for *Tmem100* CKO).

(F) Capsaicin-induced nocifensive behaviors (0.6 μg) are similar between *Tmem100* CKO and the control group (*Avil-Cre;Tmem100$^{+/+}$* mice). Time of licking and flinching: 45 ± 5.7 s in *Avil-Cre; Tmem100$^{+/+}$* vs. 53.7 ± 8.3 s in *Tmem100* CKO; n = 12 in CKO and 10 in control; p = 0.40).

(G and H) *Tmem100* CKO mice show decreased mechanical hyperalgesia but intact thermal hyperalgesia after CFA injection. One and 2 days after CFA injection, *Tmem100* CKO mice had higher mechanical thresholds than both control groups, but the response to painful thermal stimuli remained unchanged (*p < 0.05; **p < 0.01; ***p < 0.001; n = 16 for *Avil-Cre;Tmem100$^{+/+}$*; 10 for *Tmem100$^{fl/fl}$* ; 18 for *Tmem100* CKO for G; n = 9 for *Avil-Cre;Tmem100$^{+/+}$*; 10 for *Tmem100$^{fl/fl}$* ; 11 for *Tmem100* CKO for H).

(I and J) Nocifensive responses in the hot plate and tail immersion tests were intact in *Tmem100 CKO* mice. At the indicated temperatures, there was no difference in the latency between CKO and control groups (*Avil-Cre;Tmem100$^{+/+}$* mice) (n = 9 and 13 for control and CKO, respectively, in I; n = 13 and 10 for control and CKO, respectively, in J). All statistics are unpaired t tests except for (C), in which two-way ANOVA with Bonferroni's post hoc test is used. Data are presented as mean ± SEM.

percentage of DRG neurons responsive to MO and the alternative TRPA1-specific agonist cinnamaldehyde (CA) was significantly lower when *Tmem100* was eliminated (Bandell et al., 2004) (Figures 3A and S3A). Fourteen and 17% of DRG neurons from *Avil-Cre;Tmem100$^{+/+}$* mice (i.e., controls) showed responses to MO and CA, respectively, and the percentages dropped to 6% and 8% in the *Tmem100* CKO group. Conversely, the percentage of DRG neurons with TRPV1 activity remained unchanged as 31% of IB4-negative DRG neurons responded to capsaicin in both *Avil-Cre;Tmem100$^{+/+}$* and *Tmem100* CKO mice. We also used menthol as a control and observed no difference in the percentage of neurons responsive to menthol, which is mostly mediated by TRPM8 at this concentration (Bautista et al., 2006; Dhaka et al., 2007), between the control and *Tmem100* CKO neurons (Figure 3A).

Whole-cell patch-clamp recording of DRG neurons was carried out to investigate regulation of TRPA1 and TRPV1-mediated currents by Tmem100. The currents evoked by 7 and 25 μM MO (based on the dose-response curve in Figure S3B) in capsaicin (CAP)-responsive neurons were significantly smaller in DRG neurons from *Tmem100* CKO mice compared to *Avil-Cre;Tmem100$^{+/+}$* neurons (Figures 3B and 3C). This finding also showed that Tmem100 enhances TRPA1 activity.

We also examined the effect of Tmem100 on TRPV1-mediated responses. CAP (100 nM)-evoked currents in DRG neurons were not significantly different between *Avil-Cre;Tmem100$^{+/+}$* and

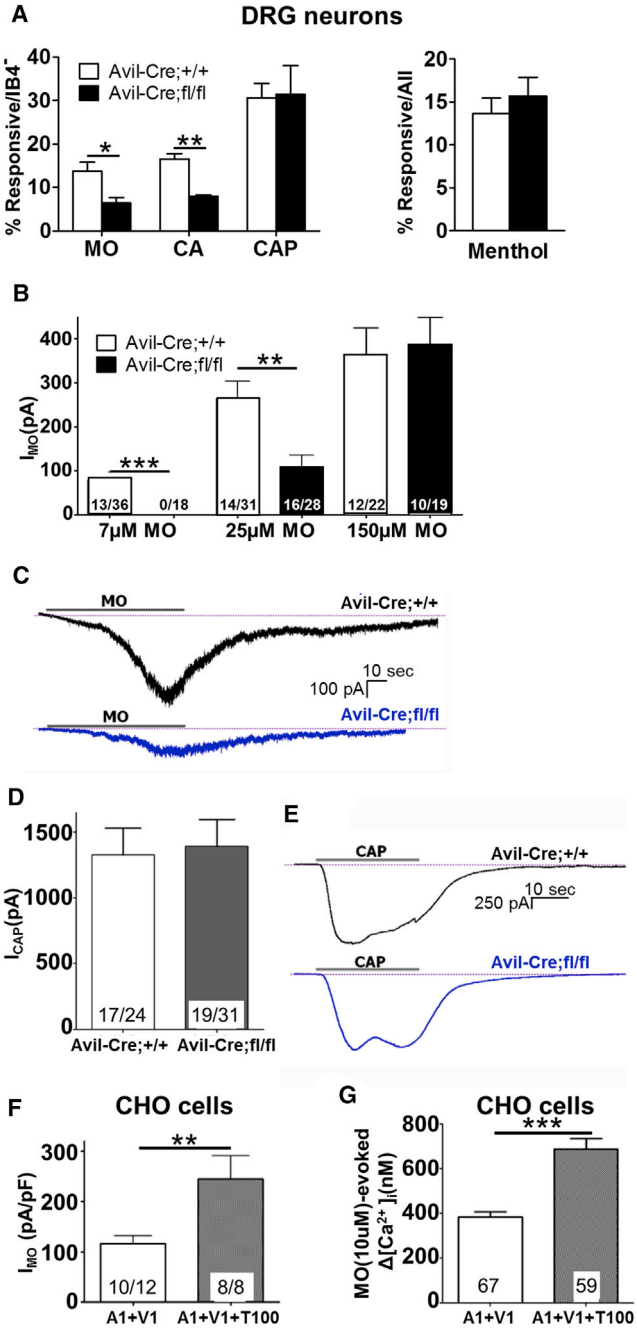

Figure 3. Tmem100 Enhances TRPA1-Mediated Responses in a TRPV1-Dependent Manner

(A) TRPA1 activity in the DRG neurons of *Tmem100* CKO mice was reduced, whereas TRPV1 activity was relatively unchanged. The percentage of neurons responding to 10 μM mustard oil (MO) and 250 μM cinnamaldehyde (CA) was lower in the CKO line, whereas the percentage of neurons responding to 100 nM capsaicin (CAP) and 100 μM menthol were similar between the CKO and control groups. (Each reagent was tested greater than three times in three mice; greater than 300 $IB4^-$ cells were assessed in the MO, CA, and CAP group, and greater than 297 cells were assessed in the menthol group. All statistics are unpaired t tests. The error bars represent SEM; *$p < 0.05$; **$p < 0.01$.)

(B) The average current induced by 7 or 25 μM MO (1 min application) is lower in DRG neurons from *Tmem100* CKO mice, whereas there is no significant difference when 150 μM MO is applied. The numbers in the columns represent the number of cells responding/ the number of cells tested. More than three mice were tested from each group; all statistics are with unpaired t tests. All error bars represent SEM; **$p < 0.01$.

(C) Representative traces of MO-induced currents from *Avil-Cre;Tmem100*$^{+/+}$ and *Avil-Cre;Tmem100*$^{fl/fl}$ mice.

(D) The average current induced by 100 nM CAP (30 s application) is similar among DRG neurons from *Tmem100* CKO and control mice. The numbers in the columns represent the number of cells responding/the number of cells tested. More than three mice were tested from each group; all statistics are unpaired t tests. The error bars represent SEM.

(E) Representative traces of CAP-induced currents from *Avil-Cre;Tmem100*$^{+/+}$ and *Avil-Cre;Tmem100*$^{fl/fl}$ mice.

(F) MO (10 μM)-gated whole-cell voltage clamp (Vh = −60 mV) current densities in TRPA1+TRPV1 (1:1)- and TRPA1+TRPV1+Tmem100 (1:1:4)-expressing CHO cells. The number of cells analyzed and those that responded are indicated within bars. The statistic is an unpaired t test (**$p < 0.01$). Error bars, SEM.

(G) MO (10 μM)-evoked Ca^{2+} influx into TRPA1+TRPV1 (1:1)- and TRPA1+TRPV1+Tmem100 (1:1:4)-expressing CHO cells. The numbers of cells responding are indicated within bars. The statistic is an unpaired t test (***$p < 0.001$). Data are presented as mean ± SEM.

Tmem100 CKO mice (Figures 3D and 3E). Therefore, Tmem100 shows no modulatory effect on TRPV1 activity.

Tmem100 Enhances TRPA1 Activity in Heterologous Expression Systems

Because both behavioral and cellular analyses suggest native Tmem100 positively regulates TRPA1, we next asked if we could reproduce a similar effect in a heterologous system. To mimic the situations in wild-type and *Tmem100*$^{-/-}$ DRG neurons, we coexpressed TRPA1 and TRPV1 in CHO cells in the presence or absence of Tmem100. MO-evoked whole-cell current density and intracellular calcium accumulation were significantly higher when Tmem100 was present with TRPA1 and TRPV1 (Figures 3F and 3G). A biotinylation assay revealed a trend of decreasing TRPA1 levels (not statistically significant) on the plasma membrane when wild-type Tmem100 was coexpressed with both TRPV1 and TRPA1, whereas TRPV1 levels on the plasma membrane remained unchanged (Figures S3D–S3F). Because the effect of Tmem100 on TRPA1 trafficking to the plasma membrane is opposite that of its enhancement of channel activity, the true effect of Tmem100 on the whole cell may be even stronger if the lowering effect on membrane trafficking of the TRPA1 channel is taken into account.

To demonstrate that Tmem100's actions can be reproduced in an alternative heterologous expression system, we coexpressed TRPA1 and TRPV1 in HEK293T cells. Tmem100 rendered 30% and 20% of cells responsive to CA and MO, respectively, whereas only 13% and 8% of cells responded to the same agonist in the control group without Tmem100. Interestingly, this enhancement was abolished when TRPV1 was replaced by TRPM8 (Figures S3G and S3H), suggesting TRPM8 does not have an inhibitory effect on TRPA1 as TRPV1 does. Moreover, Tmem100 also lowered the EC_{50} to CA by almost 3-fold compared to the control group (Figure S3J). These results suggest that Tmem100 selectively enhances TRPA1 activity at the whole-cell level. Importantly, this positive effect requires the presence of TRPV1.

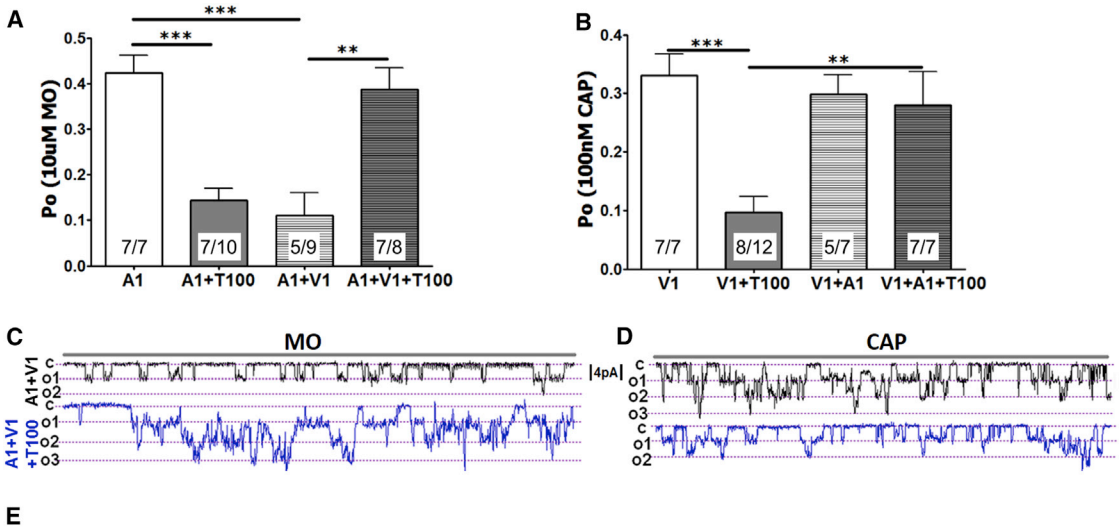

E

Drug	Mustard Oil				Capsaicin			
Expressed Genes	A1	A1+T100	A1+V1	A1+V1+T100	V1	V1+T100	A1+V1	A1+V1+T100
Single-channel slope conductance (pS)	73.6±0.9	34.9±1.8	51.9±1.7	45.1±1.6	63.5±2.0	30.0±2.9	78.7±3.8	98.1±2.6
Effect for P_o (open probability)	Decrease		Increase		Decrease		No effect	

Figure 4. Context-Dependent Regulation of Tmem100 in the TRPA1-V1 Complex

(A and B) MO (10 μM)- (A) and CAP (100 nM)-induced (B) single-channel open probability (P_o) of the main conductance at Vh = −60 mV in CHO cells expressing TRPA1 versus TRPA1+Tmem100 (T100) (1:4 molar ratio) and TRPA1+TRPV1 (1:1) versus TRPA1+TRPV1+Tmem100 (1:1:4). The configuration is cell-attached patch, and the number of cells that responded among those analyzed is indicated within bars. The statistic is one-way ANOVA with Bonferroni's post hoc test for comparison between all columns (**$p < 0.01$; ***$p < 0.001$); error bars, SEM.

(C and D) Representative single-channel recording during 5 s at Vh = −60mV for MO-gated current (C) and 4 s for CAP-gated current (D) in TRPA1+TRPV1- and TRPA1+TRPV1+Tmem100-expressing CHO cells; c is the closed state, o1, o2, and o3 show open states for three independent channels in the patch.

(E) Summary of data on single-channel conductance (pS) and effects on Po changes of Tmem100 (T100) for the given agonists and genes expressed. The values of single-channel conductance were derived from Figure S4. Data are presented as mean ± SEM.

Tmem100 Selectively Increases the Single-Channel Open Probability of the TRPA1-V1 Complex to Mustard Oil but Not Capsaicin

To analyze the effect of Tmem100 on TRPA1 and TRPV1 channel properties, we performed cell-attached single-channel recordings. Using CHO cells expressing various combinations of Tmem100, TRPA1, and TRPV1, we investigated open probabilities (Po), single-channel activity (NPo), and conductance in response to MO and CAP. The presence of TRPA1-V1 in the recording patch was confirmed with single-channel responses to both CAP and MO. When Tmem100 was coexpressed with TRPA1 and TRPV1, a substantial increase was seen in the TRPA1 Po; there was no increase in TRPA1 unitary single-channel conductance (Figures 4A, 4E, S3K, and S4E). The presence of Tmem100 also caused a higher percentage of cells to respond to MO and CA (Figures S3L and S3M). This modulation is not a dose-dependent effect based on the ratio of Tmem100 to TRPA1 or TRPV1 because the experiments with a different transfection ratio of Tmem100 still yielded similar results (Figure S3I). Interestingly, coexpression of Tmem100 with TRPA1 in the absence of TRPV1 significantly reduced the TRPA1 Po for both the main conductance and unitary single-channel conductance (Figures 4A, 4E, S4C, and S4E). Recordings of TRPV1 and TRPA1, in both heterologous expression systems and sensory neurons, exhibit multiple single-channel subconductance states (Nagata et al., 2005; Premkumar et al., 2002; Staruschenko et al., 2010). This subconductance will influence the whole-cell response; therefore, to examine the subconductance contributions, we also analyzed the effects of Tmem100 on single-channel activity (NPo) of TRPA1 and TRPV1. Figure S4A illustrates that Tmem100 regulates TRPA1 NPo in the same way it affects Po; i.e., Tmem100 increases the TRPA1 NPo in the presence of TRPV1 and reduces its activity when TRPV1 is absent.

TRPV1 single-channel Po and unitary conductance, as assessed by the application of CAP, was relatively unaffected by Tmem100 when TRPA1 was also present in patches (Figures 4B, 4E, and S4F). However, Tmem100 reduced single-channel CAP responses in CHO cells expressing TRPV1 alone; this effect was much weaker in DRG neurons (Figure S4K). Taken together, these results suggest that Tmem100 requires TRPV1 to increase intrinsic activity of TRPA1. Tmem100 inhibits the intrinsic activity of individual TRPA1 and TRPV1 channels when the two are not coexpressed.

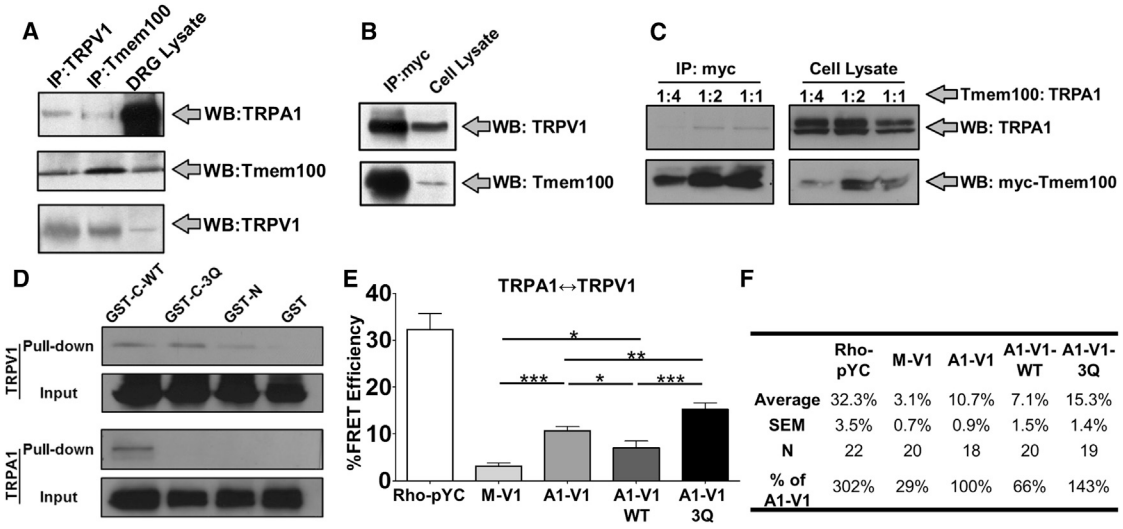

Figure 5. Tmem100 Decreases the Interaction between TRPA1 and TRPV1, whereas the Tmem100-3Q Mutant Enhances It

(A) Co-IP with Tmem100 and TRPV1 antibodies and western blotting with TRPA1, TRPV1, and Tmem100 antibodies in mouse DRG lysates. Tmem100, TRPA1, and TRPV1 form a complex in DRG neurons.

(B) Co-IP of TRPV1 and full-length myc-Tmem100 in TRPV1-expressing cells. The results show an interaction between Tmem100 and TRPV1.

(C) Co-IP of TRPA1 and full-length myc-Tmem100 in TRPA1-V1-coexpressing cells. Tmem100 binds TRPA1 at different dilutions.

(D) GST pull-down with different TRPs and fragments of Tmem100 and Tmem100-3Q proteins. TRPV1 is pulled down by the C termini of both WT Tmem100 (GST-C-WT) and Tmem100-3Q (GST-C-3Q). It is also pulled down by the N terminus of WT Tmem100 (GST-N). However, TRPA1 is pulled down only by the C terminus of WT Tmem100, whereas the Q-Q-Q mutation abolishes this interaction. The lysates from the cells expressing unconjugated GST (GST) and each TRP serve as negative controls.

(E) FRET results with TIRF microscopy for the effects of Tmem100 on TRPA1-V1 interactions. All groups were transfected with *TRPV1-CFP* and *TRPA1-YFP* except for the *Rho-pYC* (as a positive control for maximal effects of the system) and M-V1 (negative control) groups, where Rho-pYC and membrane-tethered YFP + TRPV1-CFP, respectively, were transfected instead. FRET efficiencies were highest in Tmem100-3Q-transfected cells (A1-V1-3Q), followed by the empty vector-transfected groups (A1-V1), and were lowest in cells transfected with wild-type Tmem100 (A1-V1-WT). The statistic is one-way ANOVA (*$p < 0.05$; **$p < 0.01$, ***$p < 0.001$). Data are presented as mean ± SEM.

(F) Summary of the data from (E).

Tmem100 Binds Both TRPA1 and TRPV1

To test the possibility that the functional interaction of Tmem100 with TRPA1 and TRPV1 is due to a complex assembled in sensory neurons, we performed coimmunoprecipitation (co-IP) experiments from DRG lysates. The results show that Tmem100 forms complexes with endogenous TRPA1 and TRPV1 in mouse DRG (Figure 5A). Furthermore, to investigate the contribution of each protein to complex formation, we carried out co-IP experiments using heterologous cells coexpressing Tmem100 with either TRPA1 or TRPV1. Co-IP with full-length Tmem100-myc suggested that Tmem100 forms complexes with TRPV1 and TRPA1 individually (Figures 5B and 5C). Glutathione S-transferase (GST) pull-down studies using different fragments of Tmem100 further characterized the distinct binding properties of its N and C termini. We could pull down both TRPA1 and TRPV1 separately with the C-terminal fragment of Tmem100; however, the same conditions with the N terminus of Tmem100 only pulled down TRPV1 (Figure 5D). These results indicate that Tmem100 can physically interact with TRPA1 and TRPV1.

We targeted the K-R-R sequence in the C terminus of Tmem100 because of its positive charges and conservation in vertebrates (Moon et al., 2010). To investigate the functional significance of this sequence, we mutated it to an uncharged Q-Q-Q sequence (Tmem100-3Q mutant). Interestingly, the Q-Q-Q mutation appeared to exert different effects on TRPA1 and TRPV1 binding. For TRPA1, the binding was abolished when the Q-Q-Q mutation was introduced to the C terminus (GST-C-3Q). For TRPV1, this mutation did not appear to weaken binding but instead enhanced it (Figures 5D, S5A, and S5B). These data show that although the C terminus of Tmem100 binds to both TRPA1 and TRPV1, its binding sites to these two channels are different. Therefore, Tmem100-3Q may exert distinct modulatory effects on TRPA1 and TRPV1 compared to wild-type Tmem100.

Wild-Type Tmem100 Weakens the Physical Association of TRPA1-V1, whereas Tmem100-3Q Enhances It

Förster resonance energy transfer (FRET) and total internal reflection fluorescence (TIRF) microscopy were used to search for physical evidence of the modulatory mechanisms of Tmem100 on the TRPA1-V1 complex. Cells coexpressing TRPV1-CFP and TRPA1-YFP exhibited a significantly higher FRET efficiency than cells coexpressing TRPV1-CFP and membrane-tethered YFP ("A1-V1" versus "M-V1" in Figure 5E). This implies that TRPA1 and TRPV1 form a complex in the plasma membrane. Strikingly, wild-type Tmem100 weakened the surface TRPA1-V1 interaction, decreasing the FRET efficiency by 34% compared to the efficiency of cells expressing only

TRPA1-V1. By contrast, the Tmem100-3Q mutant enhanced the TRPA1-TRPV1 interaction by 43% (Figures 5E and 5F). These data suggest that Tmem100 modulates the physical interaction of the TRPA1-TRPV1 complex, with wild-type Tmem100 and Tmem100-3Q exerting opposite effects on these interactions. In a separate FRET-TIRF experiment, we found that the physical interaction between TRPA1 and Tmem100 is further augmented in the presence of TRPV1, whereas that of TRPV1 and Tmem100 is unaffected by TRPA1 (Figures S5C and S5D). In addition, the interaction of TRPA1 and Tmem100 is weaker than that of TRPV1 and Tmem100 (comparing "V1-T100" and "A1-T100" columns in Figures S5C and S5D). The FRET data suggest preferential interactions between the three components. This result also shows that the physical interaction among the three proteins is not allosteric interaction but occurs via specific interaction domains.

Tmem100-3Q Selectively Inhibits TRPA1-Mediated Single Channel Activity in the TRPA1-V1 Complex

Further functional investigation of Tmem100-3Q revealed that mutant Tmem100 has the opposite effect of wild-type Tmem100 on TRPA1-mediated single-channel properties at −60 mV (Figures 6A–6E and S6A–S6D). We found that, in TRPA1-V1-coexpressing cells, Tmem100-3Q significantly decreased single-channel MO-evoked Po with modest alterations in unitary conductance (Figures 6A, 6E, and S6). Similarly, whole-cell MO-activated current density was significantly lower in TRPA1-V1-coexpressing cells containing Tmem100-3Q than control cells without Tmem100-3Q (Figure 6F). Similar results were obtained by calcium imaging assay (Figure 6G). Tmem100-3Q also lowered the percentage of cells that responded to MO and CA in HEK293T cells expressing both TRPA1 and TRPV1 (Figures S3L and S3M). Unlike MO responses in TRPA1-V1 cells, TRPV1-mediated single-channel activity induced by CAP in TRPA1-V1 cells was relatively unchanged in the presence of Tmem100-3Q (Figures 6B, 6D, and 6E).

Like wild-type Tmem100, Tmem100-3Q also exerts context-dependent modulatory effects on TRPA1 and TRPV1 homomers. Tmem100-3Q reduced single-channel responses of cells expressing TRPV1 alone, whereas it had no effect on TRPA1 responses in cells containing only TRPA1 (Figures 6A and 6B). CAP responses from TRPV1-expressing CHO cells showed that the addition of Tmem100-3Q lowered its Po as well as NPo (Figures 6B, S6B, and S6D). In contrast, no modulatory effect of Tmem100-3Q on TRPA1-mediated single-channel open probability (Po) or activity (NPo) was observed in TRPA1-expressing cells (Figures 6A, S6A, and S6C). In summary, these data suggest that Tmem100-3Q affects intrinsic and whole-cell TRPA1 activity only in the presence of TRPV1.

Cell-Permeable Peptides Mimicking Tmem100-3Q Attenuate TRPA1 Activity and Block Pain

To selectively attenuate TRPA1-mediated activity in both cellular and behavioral studies, we utilized a cell-permeable peptide, an approach that has been employed to effectively modulate intracellular protein activity (Koren and Torchilin, 2012). We designed and synthesized T100-Mut, a peptide that shares sequence with the C terminus of Tmem100-3Q (Figure 7A). In addition, the N terminus of this peptide was conjugated with a myristoylated group, which allows peptides to penetrate and localize to the intracellular side of the plasma membrane (Nelson et al., 2007), thereby mimicking the topology of Tmem100-3Q (Figure 8D).

At the cellular level, T100-Mut mimicked the effect of full-length Tmem100-3Q by lowering TRPA1-mediated activity in the TRPA1-V1 complex. T100-Mut pretreatment selectively decreased responses to 10 μM MO in IB4-negative DRG neurons (Figure 7B). However, the peptide had no effect on responses to 100 nM CAP in the same population (Figure 7B). The results were largely consistent in a heterologous system. T100-Mut treatment produced a 65% reduction in the percentage of cells responding to MO (Figure 7C). These results suggest that T100-Mut mainly reduced TRPA1- but not TRPV1-associated activity. We also tested a cell-permeable peptide (CPP) that shares sequence with the wild-type C terminus (T100-WT). The result shows that T100-WT does not have a modulatory effect on TRPA1-V1 complexes (Figure 7C).

We next tested whether T100-Mut has a corresponding inhibitory effect on pain behaviors. T100-Mut-injected wild-type animals showed reduced MO-induced pain behavior (Figure 7D). T100-Mut treatment significantly decreased acute nocifensive behavior (36 ± 6 s) compared to the scrambled peptide-treated group (80 ± 9 s). Mechanical hyperalgesia was also significantly attenuated by T100-Mut (Figure 7D). However, T100-Mut did not alter acute nocifensive behavior induced by CAP (Figure 7F). Similar results were obtained in the CFA model: 3 hr after T100-Mut treatment, mice showed attenuated mechanical but not thermal hyperalgesia (Figure 7E). The mechanical thresholds were significantly higher in the T100-Mut-treated group. The level of thermal hyperalgesia remained similar between these two groups. T100-Mut also alleviated mechanical hyperalgesia induced by paclitaxel (Taxol), a commonly used chemotherapeutic agent that produces TRPA1-dependent neuropathy as a side effect (Materazzi et al., 2012) (Figure 7G). Furthermore, a shortened CPP (called F2) consisting of the first 18 amino acids of the T100-Mut could produce the same inhibitory effects, whereas two other shortened CPPs that spanned different regions of the T100-Mut C terminus had no effect (Figures S7A and S7B). Together, these data suggest that the first four amino acids of the Tmem100 C terminus, i.e., "WKVR," and the 3Q mutations are essential for the inhibitory effect of TMEM100-3Q on TRPA1 in the TRPA1-V1 complex and that this effect is likely caused by an enhanced interaction of TMEM100-3Q with TRPV1. Furthermore, there was no effect of T100-Mut on MO-induced acute pain and mechanical hyperalgesia in *TRPV1*$^{-/-}$ mice (Figures 7H and 7I). We also compared the effects of T100-Mut and HC-030031, a direct TRPA1 antagonist (Eid et al., 2008), and found that T100-Mut showed comparable or better efficacy and potency of inhibiting neuropathic pain as the TRPA1 antagonist (Figures S7C and S7D). These behavioral data demonstrate that T100-Mut selectively alleviates TRPA1-associated pain and that this effect is TRPV1 dependent.

DISCUSSION

Functional interaction between TRPV1 and TRPA1 can occur in several ways (Julius, 2013). TRPV1 and TRPA1 can modulate

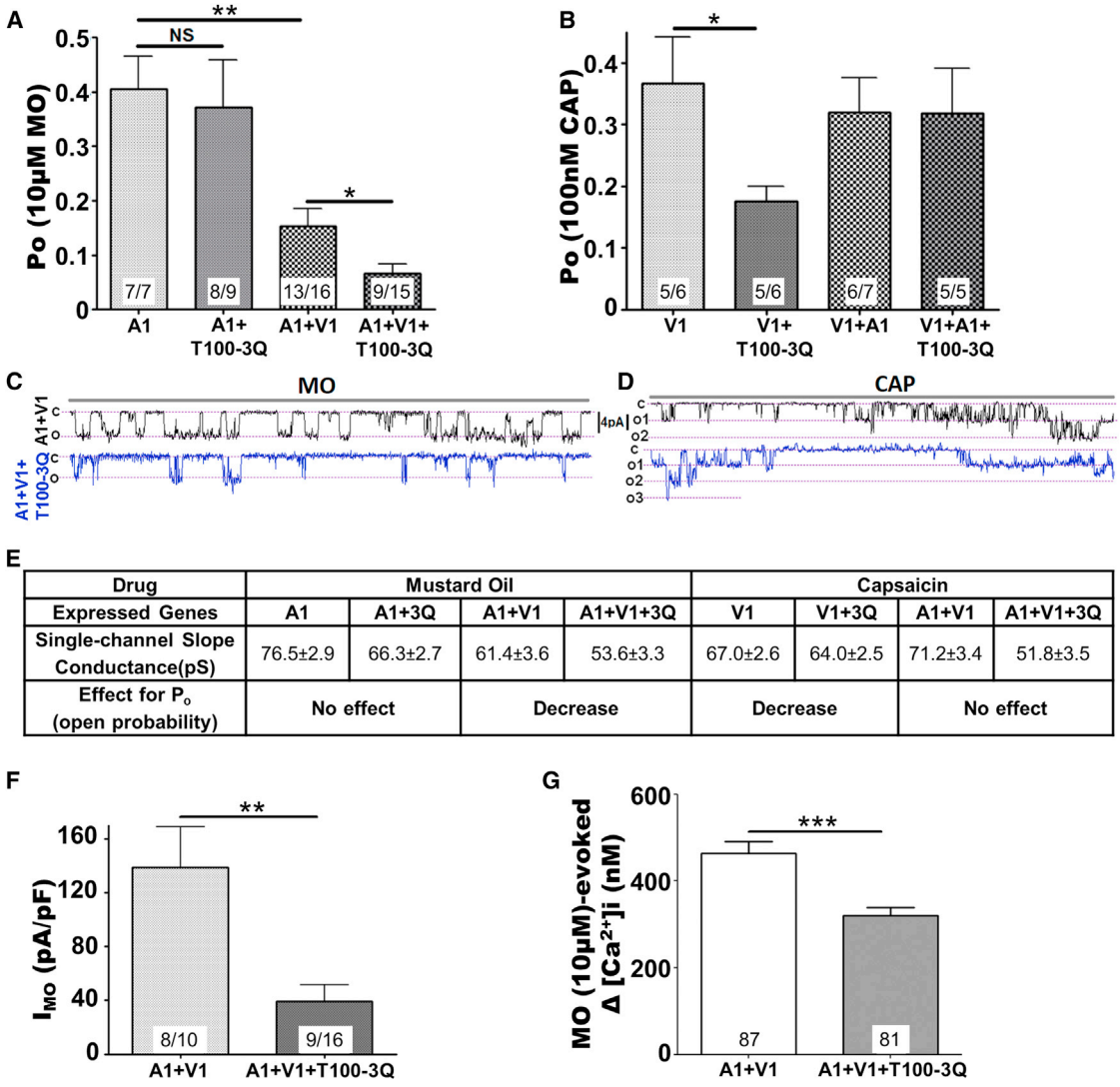

Drug	Mustard Oil				Capsaicin			
Expressed Genes	A1	A1+3Q	A1+V1	A1+V1+3Q	V1	V1+3Q	A1+V1	A1+V1+3Q
Single-channel Slope Conductance(pS)	76.5±2.9	66.3±2.7	61.4±3.6	53.6±3.3	67.0±2.6	64.0±2.5	71.2±3.4	51.8±3.5
Effect for P_o (open probability)	No effect		Decrease		Decrease		No effect	

Figure 6. Context-Dependent Regulation of Tmem100-3Q Mutant in the TRPA1-V1 Complex

(A and B) MO (10 μM)- (A) and CAP (100 nM)-induced (B) single-channel open probability (P_o) of the main conductance at Vh = −60 mV in CHO cells expressing TRPA1 versus TRPA1+Tmem100-3Q (T100-3Q) (1:4 molar ratio) and TRPA1+TRPV1 (1:1) versus TRPA1+TRPV1+Tmem100-3Q (1:1:4). The statistic is one-way ANOVA as in Figure 4; *p < 0.05; **p < 0.01; NS, no significant difference.

(C and D) Representative single-channel recording traces at Vh = −60 mV for MO- (C) and CAP-gated (D) current in TRPV1+TRPA1- versus TRPV1+TRPA1+Tmem100-3Q-expressing CHO cells. Traces are 4 s long.

(E) Summary of data on single-channel conductance (pS) and effects on P_o changes of Tmem100-3Q for the given agonists and genes expressed. The values of single-channel conductance were derived from Figure S4.

(F) MO (10 μM)-gated whole-cell voltage clamp (Vh = −60mV) current densities in TRPA1+TRPV1 (1:1)- and TRPA1+TRPV1+Tmem100-3Q (1:1:4)-expressing CHO cells. Results: 138.9 ± 29.92 pA/pF for TRPA1+TRPV1 versus 39.16 ± 12.5 pA/pF for TRPA1+TRPV1+Tmem100-3Q cells. The statistic is an unpaired t test (**p < 0.01).

(G) MO (10 μM)-evoked Ca^{2+} influx into TRPA1+TRPV1 (1:1)- and TRPA1+TRPV1+Tmem100-3Q (1:1:4)-expressing CHO cells. Results: 463.1 ± 26.8 nM for TRPA1+TRPV1 versus 321 ± 18.2 nM for TRPA1+TRPV1+Tmem100-3Q cells. The numbers of cells responding/tested are indicated within bars. The statistic is an unpaired t test (***p < 0.001). Data are presented as mean ± SEM.

each other's activity by activating intracellular pathways. For example, activation of TRPA1 can cause Ca^{2+} influx, triggering Ca^{2+}-dependent phosphatases, which, in turn, desensitize TRPV1 activity (Akopian et al., 2007). Alternatively, TRPA1-initiated Ca^{2+} influx could promote protein kinase A activity, sensitizing TRPV1 channels (Spahn et al., 2014). Behavioral experiments demonstrated that TRPA1 activation by MO leads to functional desensitization of TRPV1 responses in vivo (Jacquot et al., 2005; Ruparel et al., 2008). Similarly, activation of TRPV1 can lead to reduction of TRPA1 activity in vitro and in vivo (Akopian et al., 2007; Jacquot et al., 2005; Ruparel et al., 2008). An important element of these functional TRPV1-TRPA1

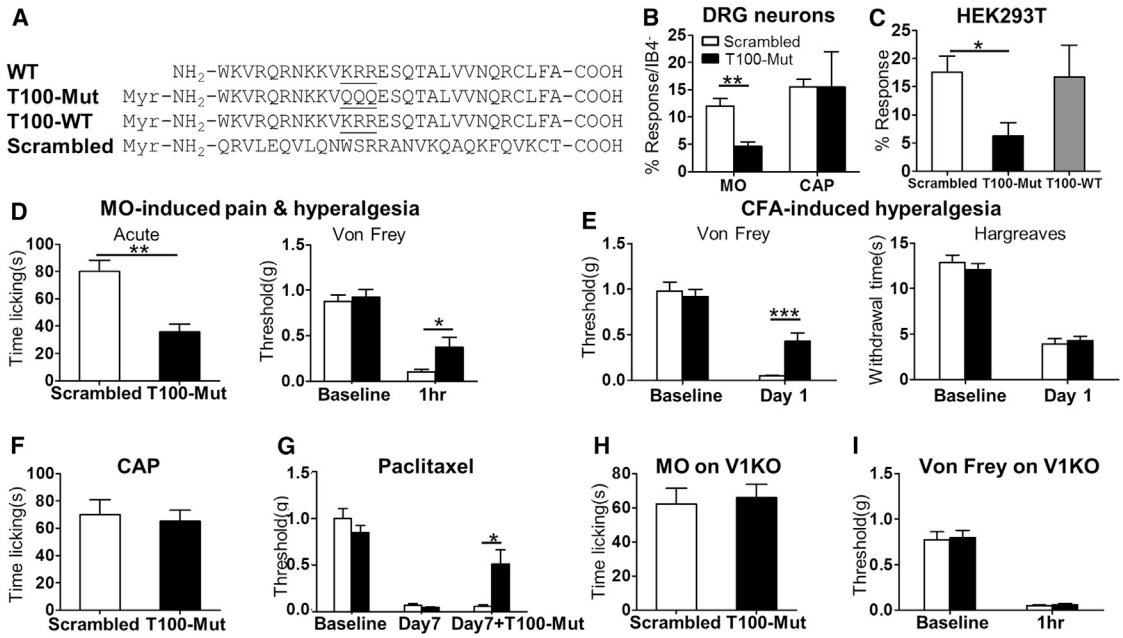

Figure 7. T100-Mut Cell-Permeable Peptide, T100-Mut, Alleviates TRPA1-Associated Pain

(A) Sequences of the cell-permeable peptide T100-Mut, scrambled peptide, T100-WT, and WT C-terminal sequence of Tmem100 (WT). Myr, myristoylation.

(B) Calcium imaging data from the T100-Mut-treated (200 nM) DRG neurons. (MO: 12% ± 1.3% in scrambled versus 4.6% ± 0.9% in T100-Mut-treated group; CAP: 16% ± 1.3% in scrambled versus 15% ± 6.5% in T100-Mut; DRG from three mice).

(C) Calcium imaging data from HEK293T cells expressing TRPA1 and TRPV1. Pretreatment of T100-Mut (200 nM) reduced the percentage of cells responsive to 500 nM MO, whereas T100-WT produced no such effect (18% ± 2.8% in scrambled, 6% ± 2.4% in T100-Mut, and 17% ± 0.6%, repeated three times, $^{*}p < 0.05$).

(D) Pretreatment with T100-Mut (5 μl of 2 mM) alleviated MO-induced acute nocifensive behavior (n = 6, $^{**}p < 0.01$) and mechanical hyperalgesia (0.1 ± 0.03 g in scrambled versus 0.4 ± 0.11 g in T100-Mut; n = 13, $^{*}p < 0.05$).

(E) Pretreatment with T100-Mut (5 μl of 2 mM) alleviated CFA-induced mechanical hyperalgesia (0.05 ± 0.0 g in scrambled versus 0.43 ± 0.1 g in T100-Mut; n = 10, $^{***}p < 0.001$) but not thermal hyperalgesia (3.9 ± 0.6 s in scrambled versus 4.3 ± 0.5 s in T100-Mut; n = 10, p = 0.63).

(F) Acute nocifensive behaviors induced by intradermal capsaicin injection (0.6 μg) were similar among the T100-Mut- and scrambled peptide-treated (2 mM) WT mice (70 ± 11 s in scrambled versus 65 ± 9 s in T100-Mut; n = 8, p = 0.73).

(G) In wild-type mice injected with paclitaxel (Taxol), mechanical hyperalgesia was observed at day 7 postinjection. Hyperalgesia was attenuated by the intradermal injection of T100-Mut (n = 7 for scrambled control peptide (open bar); n = 8 for T100-Mut peptide (black bar); $^{*}p < 0.05$).

(H and I) In TRPV1$^{-/-}$ mice, T100-Mut did not perturb MO-induced acute pain (H) and mechanical hyperalgesia (I), as observed in WT mice. (n = 8, p = 0.91 for H and 0.64 for I). All statistics are unpaired t tests and data are presented as mean ± SEM.

interactions is that the channels need to be activated sequentially.

An alternative mechanism would be the interaction of TRPV1 and TRPA1 within a complex. Indeed, a large body of evidence indicates that TRP channels are capable of assembling into channel complexes (Schaefer, 2005; Strübing et al., 2003). Physical interaction within TRP complexes may alter the conformation of channels and thus influence the biophysical and regulatory properties of each TRP channel (Xu et al., 1997). It was demonstrated that TRPV1 and TRPA1 can form a complex in heterologous expression systems and sensory neurons (Akopian et al., 2007; Fischer et al., 2014; Staruschenko et al., 2010). Formation of such a complex can strongly influence the properties of TRPA1 (Patil et al., 2011; Salas et al., 2009). The composition and function of TRPV1-TRPA1 complexes in sensory neurons is not yet clear. Requirement of TRPV1 activity for regulation within the complex is unknown too.

Our studies propose a putative TRPA1-V1 complex model in which a membrane adaptor protein, Tmem100, regulates the physical association between TRPA1 and TRPV1 (Figure 8). Our and previous studies demonstrate that TRPA1 activity is inhibited by TRPV1 when the two channels are coexpressed in the absence of Tmem100 (Figures 4A and 8A) (Salas et al., 2009). When Tmem100 is present, TRPA1 activity is potentiated in a TRPV1-dependent fashion (Figures 2, 3, and 4). The presence of Tmem100 weakens the TRPA1-V1 association by physical interaction with both channels (Figures 5E and 8B), which results in disinhibition of TRPA1 and a net-positive effect on TRPA1-associated activity in the TRPA1-V1 complex. Moreover, Tmem100-3Q (with stronger interaction with TRPV1 and no interaction with TRPA1; Figures 5 and S5) exerts the opposite effect, tightening the physical association between TRPA1 and TRPV1 (Figure 5E); TRPA1 inhibition by TRPV1 is increased (Figures 8C and 8D). The uniqueness of Tmem100 is that it not only provides a feasible model of regulation for TRPA1-V1 complexes, but also demonstrates selectivity and context dependency.

Tmem100 preferentially augments the responses to TRPA1 agonists in the TRPA1-V1 complex, whereas the responses to TRPV1 agonists remain relatively unchanged. This phenomenon is consistent from single channels all the way to the behavioral

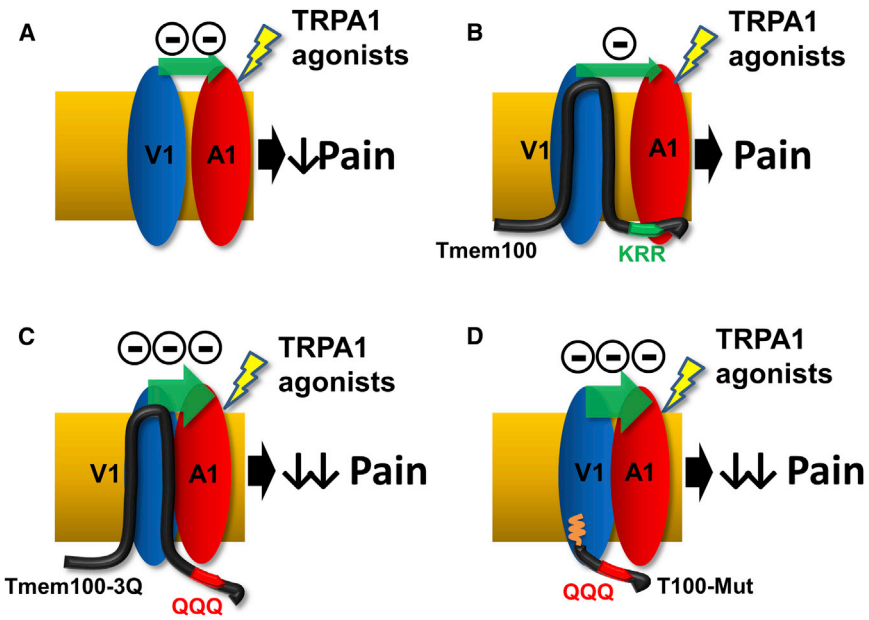

Figure 8. Model for the Modulatory Effects of TRPV1 on TRPA1

Model for the modulatory effects of TRPV1 on TRPA1 alone (A), WT Tmem100 (B), Tmem100-3Q (C), and T100-Mut CPP (D) (with myristoylated group inserted into the plasma membrane as shown by the orange wiggly line). The distance between TRPA1 and TRPV1 represents the degree of association (the smaller the distance, the stronger the association). The number of minus signs and the size of the green arrows represent the relative strength of inhibition of TRPA1 by TRPV1.

level. Electrophysiological and biochemical results indicate that Tmem100 is able to physically associate with TRPA1 and TRPV1 alone and modulate them. However, these regulatory effects are inhibitory in nature for both TRPA1 and TRPV1 homomers. Interestingly, the inhibitory effects of Tmem100 were not observed in DRG neurons and behavioral assays. One possible explanation is that most TRPA1$^+$ DRG neurons also express TRPV1; therefore, the amount of TRPA1 homomer could be minimal in DRG neurons in either normal or pathological conditions (Diogenes et al., 2007). An alternate possibility is that Tmem100 modulates channels other than the TRPA1-V1 complex and contributes to other phenotypes (Somekawa et al., 2012). We did not investigate the modulatory effects of Tmem100 on TRPV1 responses in DRG neurons and behaviors, although the data from a heterologous expression system suggested that Tmem100 may inhibit CAP-mediated responses in TRPV1$^+$/TRPA1$^-$ DRG neurons. One explanation is that Tmem100 has low expression levels in the TRPV1$^+$/TRPA1$^-$ neuronal subset (Figure 1). Further investigation is required to test this possibility.

The discovery of *Tmem100* also reconciles the inconsistent effects of TRPV1 on TRPA1-mediated currents reported in native sensory neurons versus heterologous systems (Salas et al., 2009). MO-induced currents were smaller in sensory neurons from *TRPV1*$^{-/-}$ mice. This is in contrast to the expected increase in currents because TRPV1 inhibits TRPA1 in heterologous systems. Our data provide an explanation for the underlying mechanisms. In *Tmem100*$^{-/-}$ DRG neurons, as seen in the heterologous system, TRPA1-mediated activity was lowered compared to *Tmem100*$^{+/+}$ neurons, presumably due to the inhibitory effect of TRPV1. Our heterologous studies show that Tmem100 itself also inhibits TRPA1 activity in the absence of TRPV1 (compare the "A1" and "A1+T100" columns in Figures 4A and S4A). Because TRPA1$^+$ sensory neurons from *TRPV1*$^{-/-}$ mice still express Tmem100, the MO-gated currents would be inhibited by Tmem100. This inhibition is exactly what previous studies (Salas et al., 2009) and ours (compare the open bars in Figures 7D and 7H) have found in *TRPV1*$^{-/-}$ DRG neurons and mice. Therefore, taking into account the modulatory action of Tmem100, the data collected from heterologous cells and native neurons are now consistent and suggest that the interaction between TRPV1 and TRPA1 leads to an inhibition of TRPA1 by TRPV1.

Several lines of evidence indicate that Tmem100 plays an important role in pain and inflammation. First, treatment with NSAIDs and immunosuppressants reduces its expression (Yamazaki et al., 2011). Second, inflammatory pain is reduced in *Tmem100* sensory neuron-specific knockout mice. Third, *Tmem100* is exclusively expressed in peptidergic DRG neurons, which are crucial for neurogenic inflammation (Figure 1H). Last, TRPA1 and TRPV1, both key targets of Tmem100 modulation, are critical regulators of inflammatory pain (Bautista et al., 2006; Caterina et al., 2000). Thus, an approach that interferes with this pathway will provide specificity to control pain under pathological conditions and may consequently be important in pain management.

The discovery and subsequent characterization of the T100-Mut cell-permeable peptide is a promising avenue for the management of pain. The extent of the inhibitory effect of T100-Mut is comparable to that of other potent TRPA1 antagonists (da Costa et al., 2010; McNamara et al., 2007; Petrus et al., 2007). The major advantage of this approach is to maximize the specificity and thus minimize the possible side effects of drugs by specifically targeting the TRPA1-V1 complex instead of TRP homomers expressed in other tissues. Therefore, further research on Tmem100 may lead to a better understanding of the processing, modulation, and management of pain.

EXPERIMENTAL PROCEDURES

Molecular Biology and Biochemistry

Generation of Tmem100 GFP Knockin Mouse Line

Full-length *Tmem100* cDNA from mouse DRG was cloned into the pGEM T-Easy vector (Promega) and later subcloned into the expression vector pcDNA3.1. The gene deletion constructs eliminated exon 3, which contains the entire coding region of *Tmem100*. Tmem100$^{GFP/+}$ mice were

generated using the targeting construct by the Transgenic Core Laboratory at the Johns Hopkins University. See Supplemental Information for details.

Generation of Tmem100 Conditional Knockout Mice

A BAC clone containing the entire *Tmem100* genomic sequence was purchased from Children's Hospital Oakland Research Institute and modified by recombineering (Liu et al., 2003). The final gene targeting vector contains exon 3 and a *PGK-Neo* cassette flanked by two loxP sites. For the behavioral studies, mice were crossed with WT C57/BL6 for more than five generations before mating to an *Avil*$^{+/CRE}$ line. See Supplemental Information for details.

Generation of Tmem100 Constructs

The DNA fragments corresponding to the N- (1–43) and C- (110–134) terminal regions of Tmem100 were generated by PCR amplification of *Tmem100* cDNA and subcloned into the pCMV-GST vector in frame with glutathione S-transferase (GST). The mutant forms of full-length and C terminus of Tmem100 were generated using the QuikChange Site-Directed Mutagenesis Kit (Stratagene).

Anti-Tmem100 Serum

Rabbit polyclonal antibody was raised and purified against a synthetic peptide, TEESTKENLGAPKSPTPVTC, corresponding to the N terminus of mouse Tmem100 by Proteintech Group.

Western Blot of DRG Lysate

DRG from cervical to lumbar levels were collected in 300 μl PBS and 2% SDS with protease inhibitor (Sigma P8340). The primary antibodies used were: 1:5,000 anti-Tmem100, 1:1,000 anti-TRPV1 (Santa Cruz Biotechnology, R130), and 1:1,000 anti-TRPA1 (Novus, NB110-40763). Secondary antibodies for visualization included donkey ant-rabbit and anti-mouse HRP-conjugated antibodies (GE Biosciences). See Supplemental Information for details.

Coimmunoprecipitation

DRG from all levels or CHO cells transfected with *Trpv1*, *Trpa1*, and *Tmem100-myc* were used. Whole-cell DRG or CHO cells lysates were generated 24 hr after transfection and Co-IP with either 1 μg myc antibody (EMD Millipore) or 1 μg TRPV1 antibody (Santa Cruz, R130) as described (Akopian et al., 2007). See Supplemental Information for details.

GST Pull-Down

The GST-N, GST-C fusion, and GST constructs (2 μg) were individually transfected with 2 μg of *Trpa1*, *Trpv1*, *Trpm8*, and *Trpv2* constructs into HEK293T cells with Lipofectamine 2000. The supernatants were incubated with glutathione-agarose beads (GE Bioscience). See Supplemental Information for details.

Behavioral Assays

Two- to four-month-old male mice backcrossed to C57Bl/6 mice for more than five generations were tested. All experiments were performed with the protocols approved by the Animal Care and Use Committee of Johns Hopkins University School of Medicine and University of Texas Health Science Center, San Antonio. The mice were housed in the vivarium with 12-hr-light/dark cycle, and all the behavioral tests were performed from 9 a.m. to 2 p.m. in the light cycle. The housing group was 5 at maximum. The behavioral assays were performed with the personnel blinded to the genotypes or peptides injected. See Supplemental Information for details.

Calcium Imaging

Calcium imaging assays were performed as previously described (Liu et al., 2009). Cells were loaded with 2 μM fura 2-acetomethoxy ester (Molecular Probes) for 30 min in the dark at room temperature or for 45 min at 37°C for DRG and cell lines, respectively. Intracellular calibration for calcium was performed as previously described (Akopian et al., 2007). The data were analyzed with the experimenter blinded to the genotypes or constructs transfected. See Supplemental Information for details.

Cell Culture

The DRG neurons were cultured as previously described (Liu et al., 2009). HEK293T, COS-7, and CHO cells were cultured in a medium consisting of 90% DMEM, 10% FBS, 100 U/ml penicillin, and 100 μg/ml streptomycin. Neurons were tested within 24 hr after plating onto the coverslips. See Supplemental Information for details.

Electrophysiology

Recordings were made in cell-attached single-channel or whole-cell voltage clamp configurations at 22°C –24°C from the somata of small-to-medium mouse DRG neurons (15–35 pF) or CHO cells. The baseline activities of the cells were recorded for 1–2 min prior drug applications. The durations of drug applications are noted in legends to figures. Single-channel analyses of traces were performed from the 10th to 30th s after commencing drug applications. See Supplemental Information for details.

Immunofluorescent Staining

Adult mice of 8–12 weeks old were anesthetized with pentobarbital and perfused with 20 ml 0.1 M PBS (pH 7.4; 4 degrees) as previously described (Kim et al., 2008) followed with 25 ml 4% paraformaldehyde and 14% picric acid in PBS (4 degrees). Images were obtained using the Zeiss LSM700 confocal microscope system. See Supplemental Information for details.

Live Staining

F11 cell line was transfected with 0.6 μg of either pcDNA$_{3.1}$-Tmem100-myc or pcDNA$_{3.1}$-Tmem100 +0.2 μg mCherry following Lipofectamine 2000 protocol. The samples were incubated with primary antibodies (1:200 mouse anti-c-*myc* ab, 9B11) or 1:1,000 rabbit anti-Tmem100 antibody. They were incubated with secondary antibodies (1:1,000 goat anti-mouse immunoglobulin G [IgG]-488 [Invitrogen] or goat anti-rabbit IgG-488 [Invitrogen]). See Supplemental Information for details.

Total Internal Reflection Fluorescence Microscopy and Förster Resonance Energy Transfer

Expression vectors of pEYFP-TRPA1 (YFP on C-terminal part), pECFP-TRPV1 (CFP on C-terminal part), and pEYFP-N1 were transfected into COS-7 cells with FuGENE HD (Promega E2311), as previously described (Staruschenko et al., 2010). COS-7 cells were chosen because they have flat morphology and thus suitable for TIRF-FRET analysis. Moreover, previously it has been shown that CHO and COS cells express TRPA1 and TRPV1 to the same level (Staruschenko et al., 2010). Data from fixed cells were collected in separate facilities at University of Texas Health Science Center, San Antonio, and the Johns Hopkins University, respectively. See Supplemental Information for details.

Cell-Permeable Peptides

The sequence from the last 28 amino acids of the C terminus of the Tmem100-3Q mutant protein was synthesized and myristoylated at its N terminus (myr-WKVRQRNKKVQQQESQTALVVNQRCLFA-COOH) by Twentyfirst Century Biochemicals. The scrambled peptide was synthesized with the same composition and did not resemble any known protein (myr-QRVLEQVLQNWSR RANVKQAQKFQVKCT – COOH). For the rat behavior assays, human T100-3Q (h-T100), a palmitoylated cell-permeable peptide mutated based on the C terminus of human sequence in Tmem100, was used; the sequence is Palmitoyl-WKVRQRSKKAQQQESQTALVANQRSLFA-COOH. See Supplemental Information for details.

Statistical Analysis

Error bars are presented as mean ± SEM. Numerical data in the text are presented as mean ± SEM *n* represents the number of mice, individual responding cells, or individual tests analyzed. Statistical comparisons between two groups were conducted by two-tailed, unpaired Student's t test. Multiple groups were compared and analyzed by using one-way ANOVA and Bonferroni's post hoc test (where each column was compared to all other columns). Differences between groups with genotype and time as factors were accessed by two-way ANOVA with Bonferroni's multiple comparison post hoc tests. Power analysis was used to justify the sample size. Differences were considered as statistically significant for $p < 0.05$. Representative data are from experiments that were replicated biologically at least three times with similar results.

SUPPLEMENTAL INFORMATION

Supplemental Information includes Supplemental Experimental Procedures and seven figures and can be found with this article online at http://dx.doi.org/10.1016/j.neuron.2014.12.065.

ACKNOWLEDGMENTS

We thank Dr. Bo Xiao at West China Hospital, Sichuan University, China for making the Tmem100 conditional knockout targeting construct. We thank Chip Hawkins and Holly Wellington of the Mouse ES cell Core (P30NS050274) at Johns Hopkins University School of Medicine for assistance with the generation of Tmem100 conditional knockout mice. We also thank Dr. Manuela Schmidt at the Max-Planck-Institute for Experimental Medicine in Germany for providing the anti-TRPA1 antibody, Dr. Michael Caterina at Johns Hopkins University for providing anti-TRPV1 antibody, Dr. Fan Wang at Duke University for providing Advillin-Cre mice, and Dr. Diana Bautista at University of California, Berkeley for providing F11 cell lines. This work was supported by NIH Grants (R01DE022750 and R01GM087369) to X.D., who is an Early Career Scientist of the Howard Hughes Medical Institute. This work was also supported by NIH grants (R01DE019311) to A.N.A. and (R01NS082746) N.A.J. and a NRSA Fellowship (F32NS079148) to S.M.B.

Received: June 30, 2014
Revised: November 3, 2014
Accepted: December 22, 2014
Published: January 29, 2015

REFERENCES

Akopian, A.N., Ruparel, N.B., Jeske, N.A., and Hargreaves, K.M. (2007). Transient receptor potential TRPA1 channel desensitization in sensory neurons is agonist dependent and regulated by TRPV1-directed internalization. J. Physiol. *583*, 175–193.

Bandell, M., Story, G.M., Hwang, S.W., Viswanath, V., Eid, S.R., Petrus, M.J., Earley, T.J., and Patapoutian, A. (2004). Noxious cold ion channel TRPA1 is activated by pungent compounds and bradykinin. Neuron *41*, 849–857.

Barabas, M.E., Kossyreva, E.A., and Stucky, C.L. (2012). TRPA1 is functionally expressed primarily by IB4-binding, non-peptidergic mouse and rat sensory neurons. PLoS ONE *7*, e47988.

Bautista, D.M., Jordt, S.E., Nikai, T., Tsuruda, P.R., Read, A.J., Poblete, J., Yamoah, E.N., Basbaum, A.I., and Julius, D. (2006). TRPA1 mediates the inflammatory actions of environmental irritants and proalgesic agents. Cell *124*, 1269–1282.

Caterina, M.J., Schumacher, M.A., Tominaga, M., Rosen, T.A., Levine, J.D., and Julius, D. (1997). The capsaicin receptor: a heat-activated ion channel in the pain pathway. Nature *389*, 816–824.

Caterina, M.J., Leffler, A., Malmberg, A.B., Martin, W.J., Trafton, J., Petersen-Zeitz, K.R., Koltzenburg, M., Basbaum, A.I., and Julius, D. (2000). Impaired nociception and pain sensation in mice lacking the capsaicin receptor. Science *288*, 306–313.

da Costa, D.S.M., Meotti, F.C., Andrade, E.L., Leal, P.C., Motta, E.M., and Calixto, J.B. (2010). The involvement of the transient receptor potential A1 (TRPA1) in the maintenance of mechanical and cold hyperalgesia in persistent inflammation. Pain *148*, 431–437.

Dhaka, A., Murray, A.N., Mathur, J., Earley, T.J., Petrus, M.J., and Patapoutian, A. (2007). TRPM8 is required for cold sensation in mice. Neuron *54*, 371–378.

Diogenes, A., Akopian, A.N., and Hargreaves, K.M. (2007). NGF up-regulates TRPA1: implications for orofacial pain. J. Dent. Res. *86*, 550–555.

Eid, S.R., Crown, E.D., Moore, E.L., Liang, H.A., Choong, K.C., Dima, S., Henze, D.A., Kane, S.A., and Urban, M.O. (2008). HC-030031, a TRPA1 selective antagonist, attenuates inflammatory- and neuropathy-induced mechanical hypersensitivity. Molecular pain *4*, 48-8069-8064-8048.

Fischer, M.J., Balasuriya, D., Jeggle, P., Goetze, T.A., McNaughton, P.A., Reeh, P.W., and Edwardson, J.M. (2014). Direct evidence for functional TRPV1/TRPA1 heteromers. Pflügers Archiv-European Journal of Physiology, 1–13.

Frullanti, E., Colombo, F., Falvella, F.S., Galvan, A., Noci, S., De Cecco, L., Incarbone, M., Alloisio, M., Santambrogio, L., Nosotti, M., et al. (2012). Association of lung adenocarcinoma clinical stage with gene expression pattern in noninvolved lung tissue. International journal of cancer *131*, E643–648.

Georgas, K., Rumballe, B., Valerius, M.T., Chiu, H.S., Thiagarajan, R.D., Lesieur, E., Aronow, B.J., Brunskill, E.W., Combes, A.N., Tang, D., et al. (2009). Analysis of early nephron patterning reveals a role for distal RV proliferation in fusion to the ureteric tip via a cap mesenchyme-derived connecting segment. Dev. Biol. *332*, 273–286.

Goel, M., Sinkins, W.G., and Schilling, W.P. (2002). Selective association of TRPC channel subunits in rat brain synaptosomes. J. Biol. Chem. *277*, 48303–48310.

Hasegawa, H., Abbott, S., Han, B.X., Qi, Y., and Wang, F. (2007). Analyzing somatosensory axon projections with the sensory neuron-specific Advillin gene. The Journal of neuroscience *27*, 14404–14414.

Hellwig, N., Albrecht, N., Harteneck, C., Schultz, G., and Schaefer, M. (2005). Homo- and heteromeric assembly of TRPV channel subunits. J. Cell Sci. *118*, 917–928.

Hofmann, T., Schaefer, M., Schultz, G., and Gudermann, T. (2002). Subunit composition of mammalian transient receptor potential channels in living cells. Proc. Natl. Acad. Sci. USA *99*, 7461–7466.

Jacquot, L., Monnin, J., Lucarz, A., and Brand, G. (2005). Trigeminal sensitization and desensitization in the nasal cavity: a study of cross interactions. Rhinology *43*, 93–98.

Jeske, N.A., Por, E.D., Belugin, S., Chaudhury, S., Berg, K.A., Akopian, A.N., Henry, M.A., and Gomez, R. (2011). A-kinase anchoring protein 150 mediates transient receptor potential family V type 1 sensitivity to phosphatidylinositol-4,5-bisphosphate. The Journal of neuroscience *31*, 8681–8688.

Julius, D. (2013). TRP channels and pain. Annu. Rev. Cell Dev. Biol. *29*, 355–384.

Kim, A.Y., Tang, Z., Liu, Q., Patel, K.N., Maag, D., Geng, Y., and Dong, X. (2008). Pirt, a phosphoinositide-binding protein, functions as a regulatory subunit of TRPV1. Cell *133*, 475–485.

Koren, E., and Torchilin, V.P. (2012). Cell-penetrating peptides: breaking through to the other side. Trends Mol. Med. *18*, 385–393.

Kwan, K.Y., Allchorne, A.J., Vollrath, M.A., Christensen, A.P., Zhang, D.-S., Woolf, C.J., and Corey, D.P. (2006). TRPA1 contributes to cold, mechanical, and chemical nociception but is not essential for hair-cell transduction. Neuron *50*, 277–289.

Liu, P., Jenkins, N.A., and Copeland, N.G. (2003). A highly efficient recombineering-based method for generating conditional knockout mutations. Genome Res. *13*, 476–484.

Liu, Q., Tang, Z., Surdenikova, L., Kim, S., Patel, K.N., Kim, A., Ru, F., Guan, Y., Weng, H.J., Geng, Y., et al. (2009). Sensory neuron-specific GPCR Mrgprs are itch receptors mediating chloroquine-induced pruritus. Cell *139*, 1353–1365.

Liu, Q., Weng, H.J., Patel, K.N., Tang, Z., Bai, H., Steinhoff, M., and Dong, X. (2011). The distinct roles of two GPCRs, MrgprC11 and PAR2, in itch and hyperalgesia. Sci. Signal. *4*, ra45.

Materazzi, S., Fusi, C., Benemei, S., Pedretti, P., Patacchini, R., Nilius, B., Prenen, J., Creminon, C., Geppetti, P., and Nassini, R. (2012). TRPA1 and TRPV4 mediate paclitaxel-induced peripheral neuropathy in mice via a glutathione-sensitive mechanism. Pflugers Arch. *463*, 561–569.

McMahon, S.B., and Wood, J.N. (2006). Increasingly irritable and close to tears: TRPA1 in inflammatory pain. Cell *124*, 1123–1125.

McNamara, C.R., Mandel-Brehm, J., Bautista, D.M., Siemens, J., Deranian, K.L., Zhao, M., Hayward, N.J., Chong, J.A., Julius, D., Moran, M.M., and Fanger, C.M. (2007). TRPA1 mediates formalin-induced pain. Proc. Natl. Acad. Sci. USA *104*, 13525–13530.

Moon, E.H., Kim, M.J., Ko, K.S., Kim, Y.S., Seo, J., Oh, S.P., and Lee, Y.J. (2010). Generation of mice with a conditional and reporter allele for Tmem100. Genesis *48*, 673–678.

Nagata, K., Duggan, A., Kumar, G., and García-Añoveros, J. (2005). Nociceptor and hair cell transducer properties of TRPA1, a channel for pain and hearing. J. Neurosci. *25*, 4052–4061.

Nelson, A.R., Borland, L., Allbritton, N.L., and Sims, C.E. (2007). Myristoyl-based transport of peptides into living cells. Biochemistry *46*, 14771–14781.

Patil, M.J., Belugin, S., and Akopian, A.N. (2011). Chronic alteration in phosphatidylinositol 4,5-biphosphate levels regulates capsaicin and mustard oil responses. J. Neurosci. Res. *89*, 945–954.

Petrus, M., Peier, A.M., Bandell, M., Hwang, S.W., Huynh, T., Olney, N., Jegla, T., and Patapoutian, A. (2007). A role of TRPA1 in mechanical hyperalgesia is revealed by pharmacological inhibition. Mol. Pain *3*, 40.

Premkumar, L.S., Agarwal, S., and Steffen, D. (2002). Single-channel properties of native and cloned rat vanilloid receptors. J. Physiol. *545*, 107–117.

Ruparel, N.B., Patwardhan, A.M., Akopian, A.N., and Hargreaves, K.M. (2008). Homologous and heterologous desensitization of capsaicin and mustard oil responses utilize different cellular pathways in nociceptors. Pain *135*, 271–279.

Salas, M.M., Hargreaves, K.M., and Akopian, A.N. (2009). TRPA1-mediated responses in trigeminal sensory neurons: interaction between TRPA1 and TRPV1. Eur. J. Neurosci. *29*, 1568–1578.

Schaefer, M. (2005). Homo- and heteromeric assembly of TRP channel subunits. Pflugers Archiv: European journal of physiology *451*, 35–42.

Schmidt, M., Dubin, A.E., Petrus, M.J., Earley, T.J., and Patapoutian, A. (2009). Nociceptive signals induce trafficking of TRPA1 to the plasma membrane. Neuron *64*, 498–509.

Somekawa, S., Imagawa, K., Hayashi, H., Sakabe, M., Ioka, T., Sato, G.E., Inada, K., Iwamoto, T., Mori, T., Uemura, S., et al. (2012). Tmem100, an ALK1 receptor signaling-dependent gene essential for arterial endothelium differentiation and vascular morphogenesis. Proc. Natl. Acad. Sci. USA *109*, 12064–12069.

Spahn, V., Stein, C., and Zöllner, C. (2014). Modulation of transient receptor vanilloid 1 activity by transient receptor potential ankyrin 1. Mol. Pharmacol. *85*, 335–344.

Staruschenko, A., Jeske, N.A., and Akopian, A.N. (2010). Contribution of TRPV1-TRPA1 interaction to the single channel properties of the TRPA1 channel. J. Biol. Chem. *285*, 15167–15177.

Story, G.M., Peier, A.M., Reeve, A.J., Eid, S.R., Mosbacher, J., Hricik, T.R., Earley, T.J., Hergarden, A.C., Andersson, D.A., Hwang, S.W., et al. (2003). ANKTM1, a TRP-like channel expressed in nociceptive neurons, is activated by cold temperatures. Cell *112*, 819–829.

Strübing, C., Krapivinsky, G., Krapivinsky, L., and Clapham, D.E. (2001). TRPC1 and TRPC5 form a novel cation channel in mammalian brain. Neuron *29*, 645–655.

Strübing, C., Krapivinsky, G., Krapivinsky, L., and Clapham, D.E. (2003). Formation of novel TRPC channels by complex subunit interactions in embryonic brain. J. Biol. Chem. *278*, 39014–39019.

Venkatachalam, K., and Montell, C. (2007). TRP channels. Annu. Rev. Biochem. *76*, 387–417.

Woolf, C.J., and Costigan, M. (1999). Transcriptional and posttranslational plasticity and the generation of inflammatory pain. Proc. Natl. Acad. Sci. USA *96*, 7723–7730.

Xu, X.-Z.S., Li, H.-S., Guggino, W.B., and Montell, C. (1997). Coassembly of TRP and TRPL produces a distinct store-operated conductance. Cell *89*, 1155–1164.

Yamazaki, T., Muramoto, M., Okitsu, O., Morikawa, N., and Kita, Y. (2011). Discovery of a novel neuroprotective compound, AS1219164, by high-throughput chemical screening of a newly identified apoptotic gene marker. Eur. J. Pharmacol. *669*, 7–14.

Neuron

Supplemental Information

Tmem100 Is a Regulator of TRPA1-TRPV1 Complex and Contributes to Persistent Pain

Hao-Jui Weng, Kush N. Patel, Nathaniel A. Jeske, Sonya M. Bierbower, Wangyuan Zou, Vinod Tiwari, Qin Zheng, Zongxiang Tang, Gary C.H. Mo, Yan Wang, Yixun Geng, Jin Zhang, Yun Guan, Armen N. Akopian, and Xinzhong Dong

SUPPLEMENTARY INFORMATION (7 figures and methods):

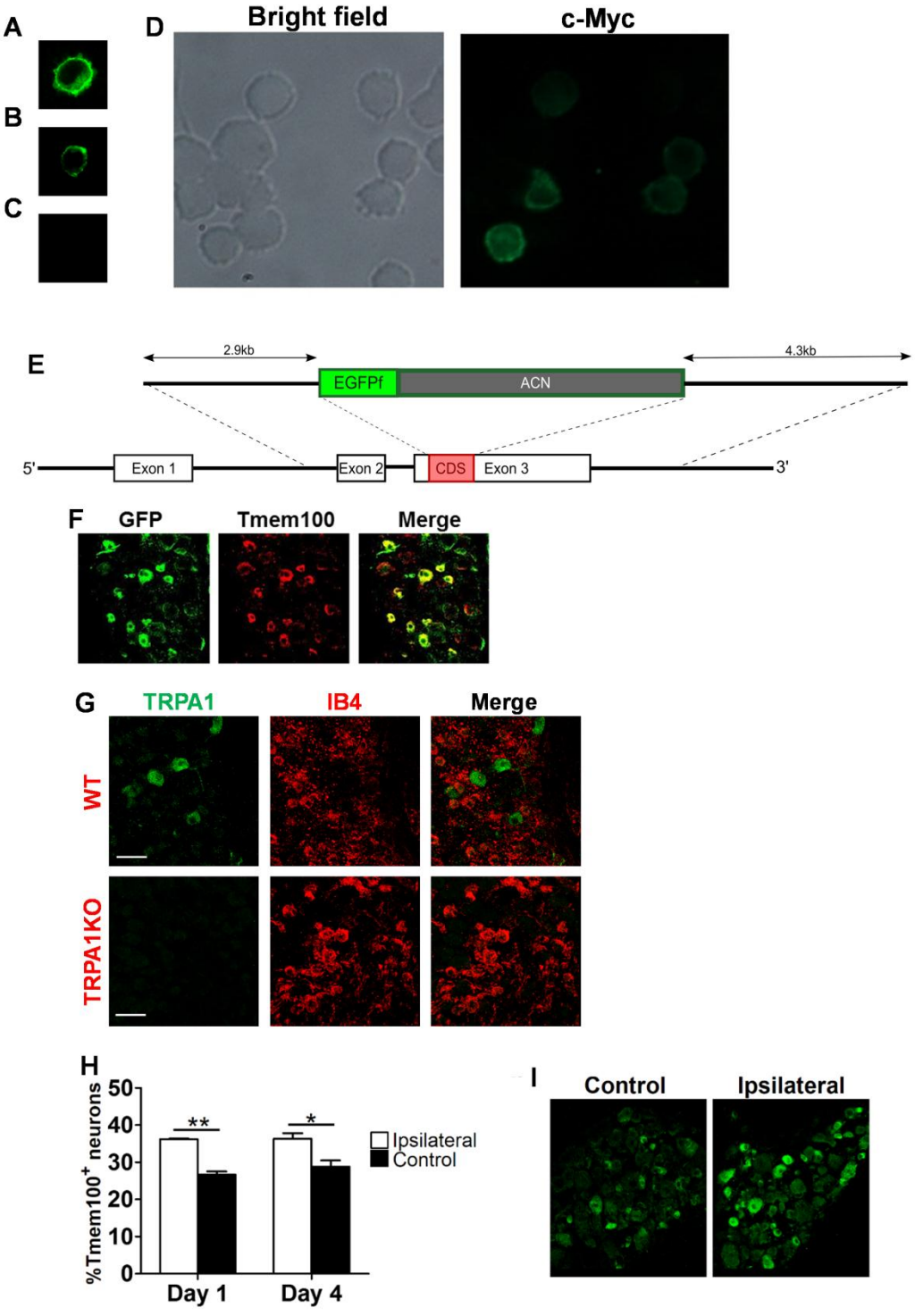

Figure S1. Related Figure 1. (**A**-**C**) Tmem100-myc signal was only visible in the plasma membrane when F11 cell lines transfected with a *Tmem100-myc* construct were treated with detergent (A). Similar results were obtained in *Tmem100*-transfected cell lines treated with an anti-Tmem100 antibody targeting the N-terminus (B). No signal was detected without detergent treatment (C). (**D**) Comparison of bright field image and c-myc staining of F11 cell lines transfected with Tmem100-myc suggested that Tmem100 primarily localizes to the plasma membrane (134 total cells were analyzed). **(E**,**F)** Design of the *Tmem100*$^{+/GFP}$ mouse line. (**E**) Tmem100 GFP knock-in strategy. The open reading frame (CDS) of Tmem100 was replaced with a targeting construct containing farnesylated enhanced GFP and the ACE promoter-Cre recombinase-Neomycin selection cassette. (**F**) Double staining of anti-GFP (green) and anti-Tmem100 (red) antibodies in *Tmem100*$^{GFP/+}$ mice confirmed GFP is a surrogate marker for Tmem100 in DRG. (**G**) Double staining of TRPA1 and IB4 in DRG. Our anti-TRPA1 antibody is specific as there is no appreciable level of background signal in DRG from TRPA1 KO mice. Moreover, TRPA1 is not expressed in IB4^{+} neurons. (**H**,**I**) Tmem100 is upregulated in the DRG neurons after inflammation. (**H**) The percentage of Tmem100-expressing neurons in L4 DRG was increased in the CFA model at days 1 and 4 compared to L4 DRG neurons on the contralateral side (control). (DRG from 3 mice, **p<0.01 at day 1; *p<0.05 at day 4.) (**I**) Immunofluorescent staining with anti-Tmem100 antibody in the L4 DRG at day 1. All data were analyzed using Student's unpaired *t*-test. All bars are presented as mean ± SEM.

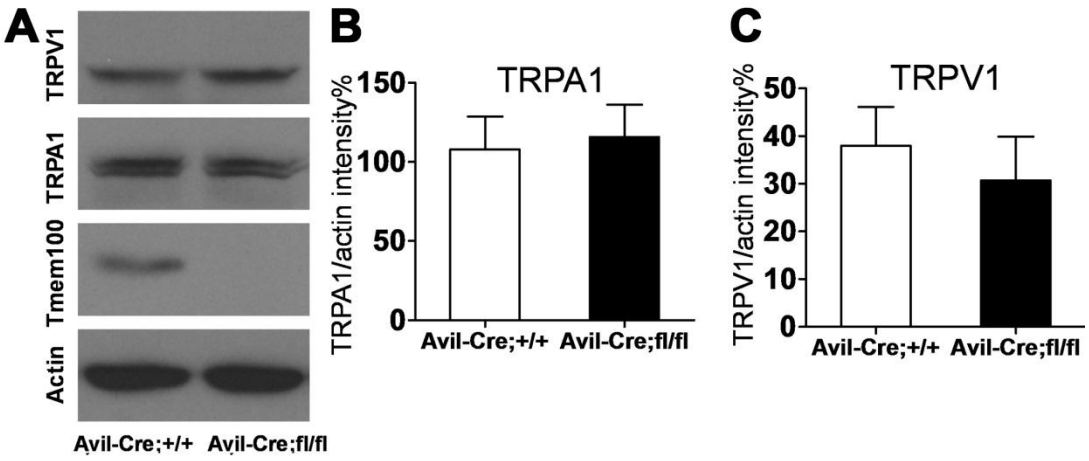

D

Marker	Genotype	Positive	Total	Percentage
CGRP	Avil-Cre; Tmem100$^{+/+}$	779	2680	28.9±2.7%
	Avil-Cre; Tmem100$^{GFP/fl}$	881	3070	28.6±1.2%
TRPV1	Avil-Cre; Tmem100$^{+/+}$	804	3238	24.3±2.5%
	Avil-Cre; Tmem100$^{GFP/fl}$	629	2871	22.0±2.2%
NF200	Avil-Cre; Tmem100$^{+/+}$	888	2399	37.3±1.2%
	Avil-Cre; Tmem100$^{GFP/fl}$	917	2598	35.4±2.1%

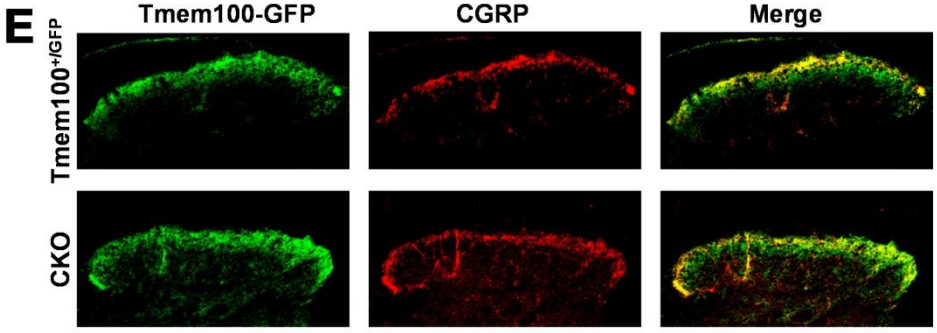

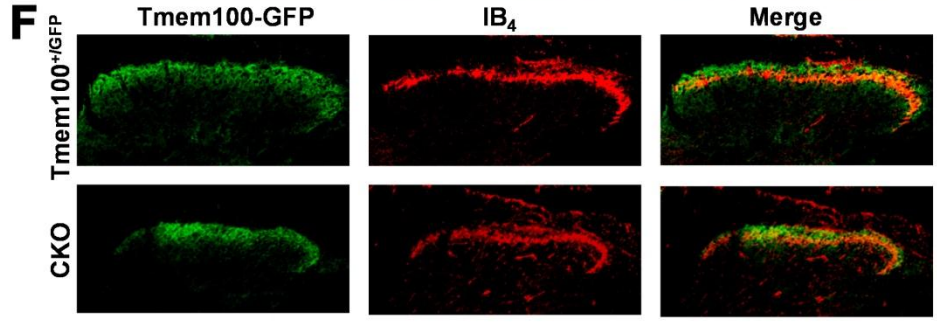

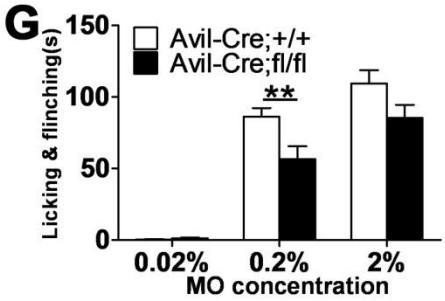

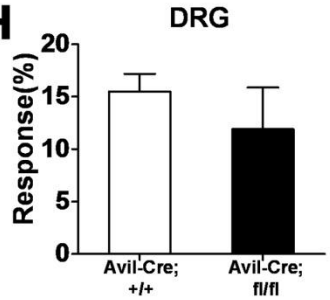

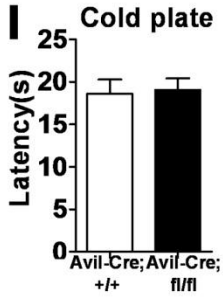

Figure S2. Related Figure 2. TRPA1 and TRPV1 levels are not altered in DRG from Tmem100 CKO mice (**A**-**C**). (**A**) Western blots using anti-TRPV1, -TRPA1, -Tmem100, and -actin antibodies from *Avil-Cre;Tmem100*$^{+/+}$ and *Avil-Cre;Tmem100*$^{fl/fl}$ (Tmem100 CKO) mice. (**B**) Pooled results of TRPA1/actin band intensities. (n=8; p=0.79; 108 ± 21 in *Avil-Cre;Tmem100*$^{+/+}$ and 116 ± 20 in Tmem100 CKO). (**C**) Pooled results of TRPV1/actin band intensities. (n=8; p=0.58; 38 ± 8 in *Avil-Cre;Tmem100*$^{+/+}$ and 31 ± 9 in Tmem100 CKO). (**D**-**F**) Developmental and morphological defects were not observed in Tmem100 conditional knockout (Tmem100 CKO) mice. (**D**) Immunofluorescent staining of DRG markers in *Avil-Cre; Tmem100*$^{GFP/fl}$ mice. None of the markers tested showed evidence of cell type-specific defects in mice lacking *Tmem100* in their primary sensory neurons. (n>3 for each marker; 8-week-old male). (**E**) Double staining of GFP (green) and CGRP (red) in the lumbar spinal cord of adult mice. (**F**) Double staining of GFP (green) and IB_4 (red) in the lumbar spinal cord of adult mice. (**G**) The acute pain phenotype induced by MO is dose-dependent. n=6 for 0.02%, 13 and 11 for *Avil-Cre;+/+* and *Avil-Cre;fl/fl* for 0.2%, and 9 and 6 for *Avil-Cre;+/+* and *Avil-Cre;fl/fl* for 2%. **p<0.01. All data were analyzed using Student's unpaired *t*-test. All bars are presented as mean ± SEM. (**H**,**I**) Cold-induced activities are not altered in *Tmem100*-deficient mice. (**H**) The percentage of DRG neurons activated by the temperature cooling from 22.5 to 13.8 °C with bath perfusion is not significantly different from *Avil-Cre;Tmem100*$^{+/+}$ and *Avil-Cre;Tmem100*$^{fl/fl}$ groups. (n=19; 16±2 in *Avil-Cre;Tmem100*$^{+/+}$ and 12±4 in *Avil-Cre;Tmem100*$^{fl/fl}$; p=0.41). (**I**) Acute pain evoked by the cold plate of zero degree is not altered in *Tmem100*-deficient mice. n=7. All data were analyzed using student's *t*-test. All bars are presented as mean ± SEM.

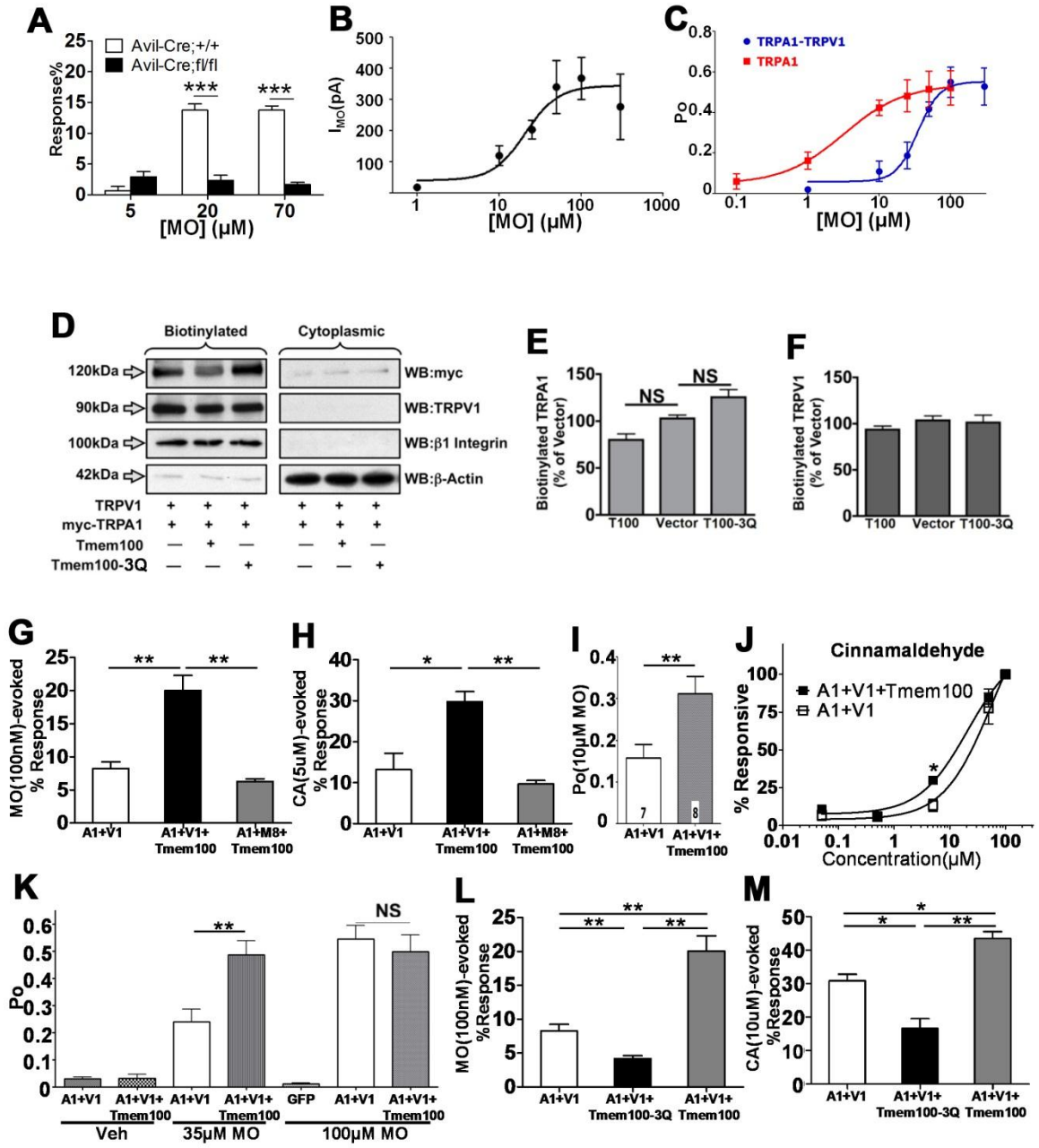

Figure S3. Related Figure 3. Dose-response curves of MO in DRG neurons and a heterologous system (**A**-**C**). (**A**) Calcium imaging of *Avil-Cre; Tmem100*$^{+/+}$ and *Avil-Cre; Tmem100*$^{fl/fl}$ DRG neurons with MO of different concentrations. n=3, 6, and 9 for 5, 20, and 70 μM, respectively. ***p<0.001. Student's *t*-test was applied for analysis. (**B**) Whole-cell recording of DRG neurons with different concentration of MO (n=7, 10, 12, 10, 12 and 9 for 1, 10, 25, 50, 100 and 300 μM). (**C**) Single-channel recording of CHO

cells expressing TRPA1 and TRPV1 or TRPA1 only, respectively (n=6, 7, 10, 10, 10, 9 and 9 for 0.1, 1, 10, 25, 50, 100 and 300 μM). Tmem100 does not significantly affect TRPA1 and TRPV1 membrane trafficking (**D**-**F**). (**D**) Biotinylation assays of CHO cells expressing myc-TRPA1, TRPV1, and either Tmem100 or Tmem100-3Q mutant. Beta1 integrin and beta-actin were used as positive controls for the biotinylated membrane and cytoplasmic fractions, respectively. (**E**) Level of biotinylated fraction of TRPA1. The TRPA1/beta1 integrin ratio was calculated and normalized to the ratio from the group transfected with myc-TRPA1 and TRPV1 only (marked as vector). Compared to the vector group, the results did not suggest a significant difference in wild-type (WT) Tmem100-transfected (T100) or Tmem100-3Q mutant-transfected cells (T100-3Q). However, the data suggest a trend towards decreased surface levels of TRPA1 in the presence of Tmem100 and increased surface levels of TRPA1 with Tmem100-3Q mutant co-expression. (**F**) Level of biotinylated portion of TRPV1. The results were analyzed in the same manner as Figure (E). The data suggest that WT Tmem100 and Tmem100-3Q mutant do not alter trafficking of TRPV1 to the surface (n=4 for (E) and (F); one-way ANOVA with Bonferroni post hoc was performed for Figures (E) and (F); NS: non-significant). TRPA1 activity evoked by MO and CA is also enhanced in the presence of Tmem100 in an alternative expression system: HEK293T cells (**G**-**M**). (**G**,**H**) TRPV1 is required for the enhancing effect of Tmem100 on TRPA1 activity. In TRPA1-V1-expressing HEK293T cells, Tmem100 increased the percentage of cells that respond to 100 nM MO and 5 μM CA. This enhancing effect of Tmem100 was abolished when TRPV1 was replaced with TRPM8, showing no interaction between TRPA1 and TRPM8. The activation of TRPA1 was monitored with calcium imaging. Each group was tested

greater than 3 times; *p<0.05; **p<0.01. The statistic is one-way ANOVA with Bonferroni's post-hoc test. All error bars represent SEM. The baseline 340/380 ratios for the cells tested were not drastically different (TRPA1+V1: 1.1 ± 0.03; TRPA1+V1+Tmem100: 1.1 ± 0.04; TRPA1+TRPM8+Tmem100: 0.95 ± 0.04). (**I**) Single-channel recording of CHO cells expressing TRPA1+TRPV1 with or without Tmem100 at a ratio of 1:1:1. Numbers of responsive cells are marked within bars. (**J**) Tmem100 increases the potency of TRPA1 activity in cells expressing both TRPA1 and TRPV1. In a heterologous system, Tmem100 lowered the EC_{50} of CA (EC_{50}=21 μM in A1+V1+Tmem100 and 57 μM in A1+V1; each concentration was tested more than 3 times). *p<0.05. (**K**) Single-channel recording of the CHO cells expressing TRPA1+TRPV1 with or without Tmem100 under different concentration of MO. n=5-8/trial. **p<0.01; NS, not significant. (**L**,**M**) Calcium imaging in HEK293T cells expressing TRPA1 and TRPV1. The percentage of cells that respond to 100 nM MO and 10 μM CA was significantly lower in the Tmem100-3Q-transfected group compared with the group lacking Tmem100-3Q (repeated 3 times; *p<0.05, **p<0.01). The statistic is one-way ANOVA with Bonferroni's post-hoc test; *p<0.05, **p<0.01. All error bars represent SEM.

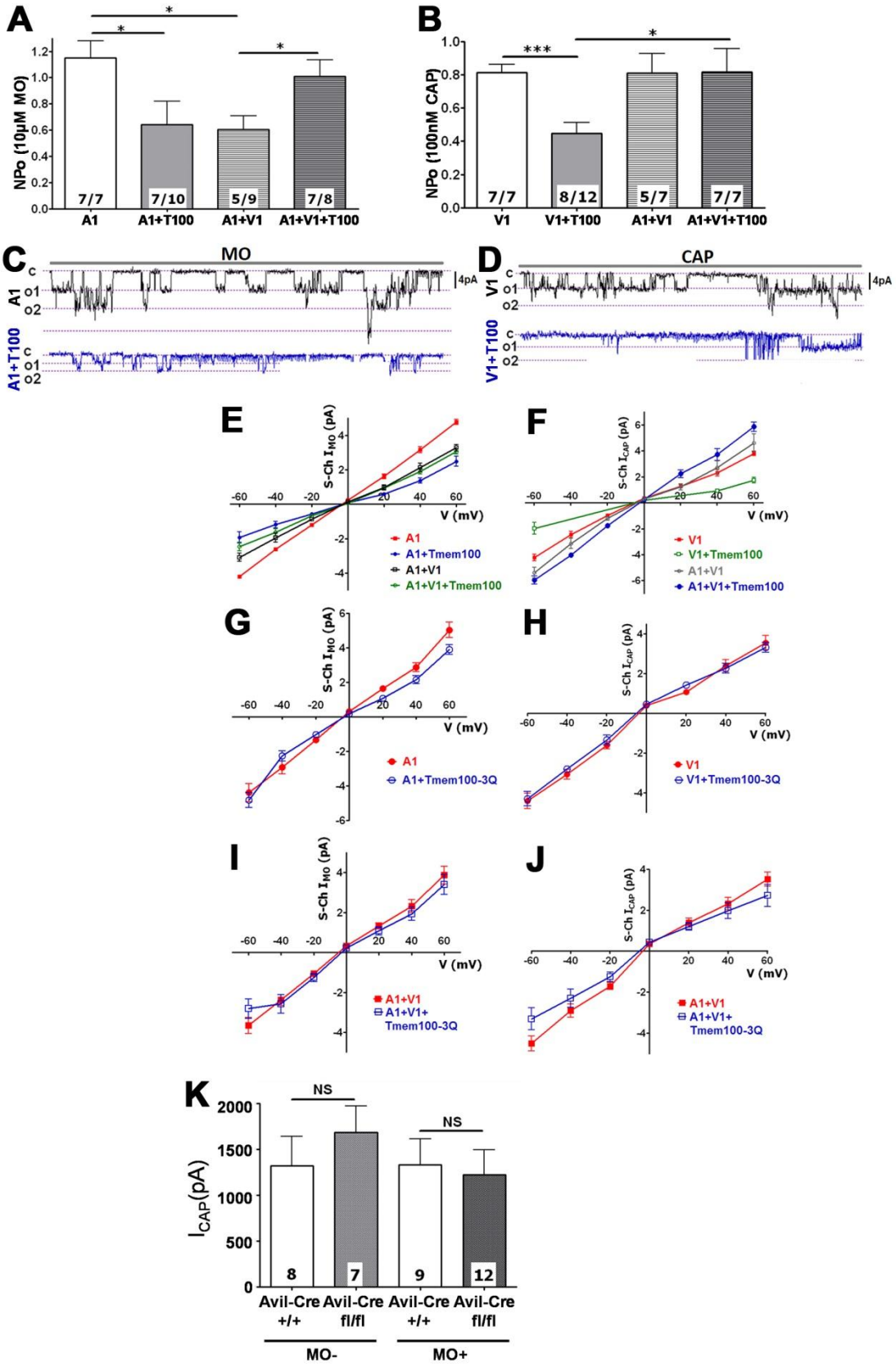
A
NPo (10μM MO)
7/7
7/10
5/9
7/8
A1
A1+T100
A1+V1
A1+V1+T100
B
NPo (100nM CAP)
7/7
8/12
5/7
7/7
V1
V1+T100
A1+V1
A1+V1+T100
C
MO
A1
A1+T100
4pA
D
CAP
V1
V1+T100
4pA
E
S-Ch I_MO (pA)
V (mV)
A1
A1+Tmem100
A1+V1
A1+V1+Tmem100
F
S-Ch I_CAP (pA)
V (mV)
V1
V1+Tmem100
A1+V1
A1+V1+Tmem100
G
S-Ch I_MO (pA)
V (mV)
A1
A1+Tmem100-3Q
H
S-Ch I_CAP (pA)
V (mV)
V1
V1+Tmem100-3Q
I
S-Ch I_MO (pA)
V (mV)
A1+V1
A1+V1+ Tmem100-3Q
J
S-Ch I_CAP (pA)
V (mV)
A1+V1
A1+V1+ Tmem100-3Q
K
I_CAP(pA)
NS
NS
8
7
9
12
Avil-Cre +/+
Avil-Cre fl/fl
Avil-Cre +/+
Avil-Cre fl/fl
MO-
MO+

Figure S4. Related Figure 4. Context-dependent regulation of Tmem100 in the TRPA1-V1 complex (**A**-**D**). (**A,B**) MO (10 μM)- (A) and CAP (100 nM)-induced (B) single-channel activity (NP_o) at Vh=-60 mV in CHO cells expressing TRPA1 vs. TRPA1+Tmem100 (1:4 molar ratio) and TRPA1+TRPV1 (1:1) vs. TRPA1+TRPV1+Tmem100 (1:1:4). NP_o measurements accounted for all recorded conductance, including main and sub-conductance. The configuration is cell-attached patch, and the number of patches that responded among those analyzed is indicated within bars. NP_o: MO 0.6±0.11 for TRPA1+TRPV1 vs. 1.05±0.14 for TRPA1+TRPV1+Tmem100 CHO cells; 1.15±0.15 for TRPA1 vs. 0.64±0.18 for TRPA1+Tmem100 CHO cells. CAP- 0.81±0.12 for TRPA1+TRPV1 vs. 0.82±0.14 for TRPA1+TRPV1+Tmem100 CHO cells; 0.81±0.07 for TRPV1 vs. 0.45±0.1 for TRPV1+Tmem100 cells. The statistic is unpaired *t*-test and one-way ANOVA with Bonferroni's post-hoc test (*$p<0.05$; ***$p<0.001$). All error bars represent SEM. (**C,D**) Representative single-channel recording during 5 sec at Vh=-60 mV for MO-gated current (C) and 4 sec for CAP-gated current (D) in TRPA1- and TRPA1+Tmem100-expressing CHO cells. Traces are 4 sec long, and the proteins expressed are indicated below the traces. Vertical bars to the right of the traces represent 4 pA; c is the closed state; o1, o2, and o3 show open states for 3 independent channels in the patch. Characterization of single channel current-voltage relationships in the presence and absence of Tmem100 and Tmem100-3Q mutant (**E**-**J**). (**E**,**G**,**I**) Mustard oil (MO; 10 μM)-gated single channel current-voltage relationship (I-V) in CHO cells expressing TRPA1, TRPA1+Tmem100 (1:4 molar ratio), TRPA1+TRPV1 (1:1), or TRPA1+TRPV1+Tmem100 (1:1:4) (E); TRPA1 and TRPA1+Tmem100-3Q (1:4) (G);

TRPA1+TRPV1 (1:1) and TRPA1+TRPV1+Tmem100-3Q (1:1:4) (I). Configuration is cell-attached patch. TRPA1 and TRPV1 co-expression in the patches was confirm by responses to both MO and CAP. I-V is presented for main single-channel conductance. Number of cells recorded: n=5-8. (**F**,**H**,**J**) CAP (100 nM)-gated single channel I-V relationship in CHO cells expressing TRPV1, TRPV1+Tmem100 (1:4), TRPA1+TRPV1 (1:1) and TRPA1+TRPV1+Tmem100 (1:1:4) (F); TRPV1 and TRPV1+Tmem100-3Q (1:4) (H); TRPA1+TRPV1 (1:1), or TRPA1+TRPV1+Tmem100-3Q (1:1:4) (J). The configuration is cell-attached patch. CHO cells co-expressing TRPA1 and TRPV1 responded to both CAP and MO. I-V is presented for main single-channel conductance. Number of cells recorded: n=5-7. Whole cell recording of capsaicin (100 nM)-evoked currents in MO (50 μM)-unresponsive (MO-) and -responsive (MO+) DRG neurons from *Avil-Cre;Tmem100*$^{+/+}$ and *Avil-Cre;Tmem100*$^{fl/fl}$ mice (**K**). The numbers in the boxes represent the numbers of capsaicin responsive neurons tested. All bars are presented as mean ± SEM.

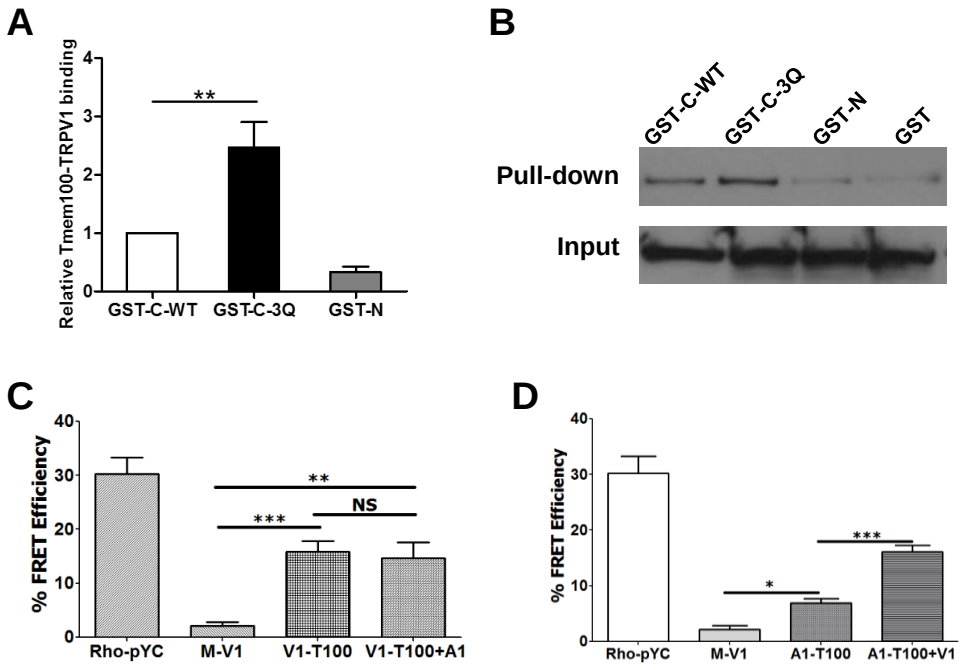

Figure S5. Related Figure 5. Interaction among Tmem100, TRPA1, and TRPV1. (**A**) Quantification of GST pull-down for the C-terminus and TRPV1. Increased association between TRPV1 and the C terminus in Tmem100-3Q was observed. n=4, **p<0.01. (**B**) GST pull-down of TRPV1 with different fragments of Tmem100 tagged with GST. TRPV1 pull-down is enhanced in the GST-C-3Q group compared to the GST-C-WT group. (**C**) FRET-TIRF measurement of the interaction among TRPV1 and Tmem100 (T100). The interaction between Tmem100 and TRPV1 is not altered by the addition of TRPA1. (**D**) FRET-TIRF measurement of the interaction among TRPA1 and Tmem100 (T100). The interaction between TRPA1 and Tmem100 is significantly increased with the presence of TRPV1. Similar to the experiments in Figure 5, the Rho-pYC was used as a positive control for maximal effects of the system, and M-V1 was a negative control. *p<0.05, **p<0.01, ***p<0.001. All bars are presented as mean ± SEM.

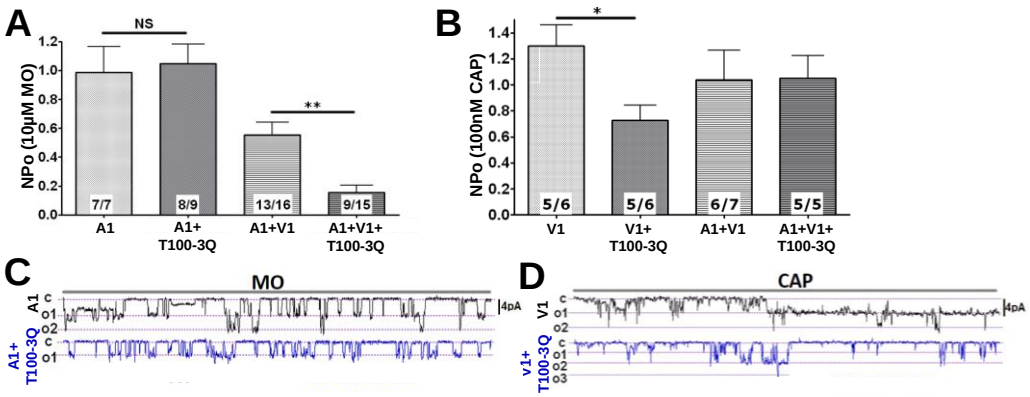

Figure S6. Related Figure 6. Context-dependent regulation of Tmem100-3Q in the TRPA1-V1 complex. (**A**,**B**) MO (10 μM)- (A) and CAP (100 nM)-induced (B) single-channel activity (NP_o) at Vh=-60 mV in CHO cells expressing TRPA1 vs. TRPA1+Tmem100-3Q (T100-3Q) (1:4 molar ratio) and TRPA1+TRPV1 (1:1) vs. TRPA1+TRPV1+Tmem100-3Q (1:1:4). NP_o: MO 0.55±0.09 for TRPA1+TRPV1 vs. 0.16±0.06 for TRPA1+TRPV1+Tmem100-3Q CHO cells; 0.98±0.18 for TRPA1 vs. 1.05±0.14 for TRPA1+Tmem100-3Q cells. CAP 1.04±0.23 for TRPA1+TRPV1 vs. 1.08±0.17 for TRPA1+TRPV1+Tmem100-3Q cells; 1.3±0.16 for TRPV1 vs. 0.73±0.12 for TRPV1+Tmem100-3Q cells. The statistic is unpaired t-test and one-way ANOVA with Bonferroni's post-hoc test (*$p<0.05$; **$p<0.01$; NS: no significant difference). All error bars represent SEM. (**C,D**) Representative single-channel recording traces at Vh=-60 mV for MO-gated current in TRPA1 and TRPA1+Tmem100-3Q-expressing CHO cells (C) and CAP-gated current in TRPV1 and TRPV1+Tmem100-3Q-expressing CHO cells (D). Traces are 4 sec long, and protein expression is indicated below the traces. Vertical bars on the right side of the traces represent 4 pA; c is the closed state; o1, o2, and o3 show open states for 3 independent channels in the patch.

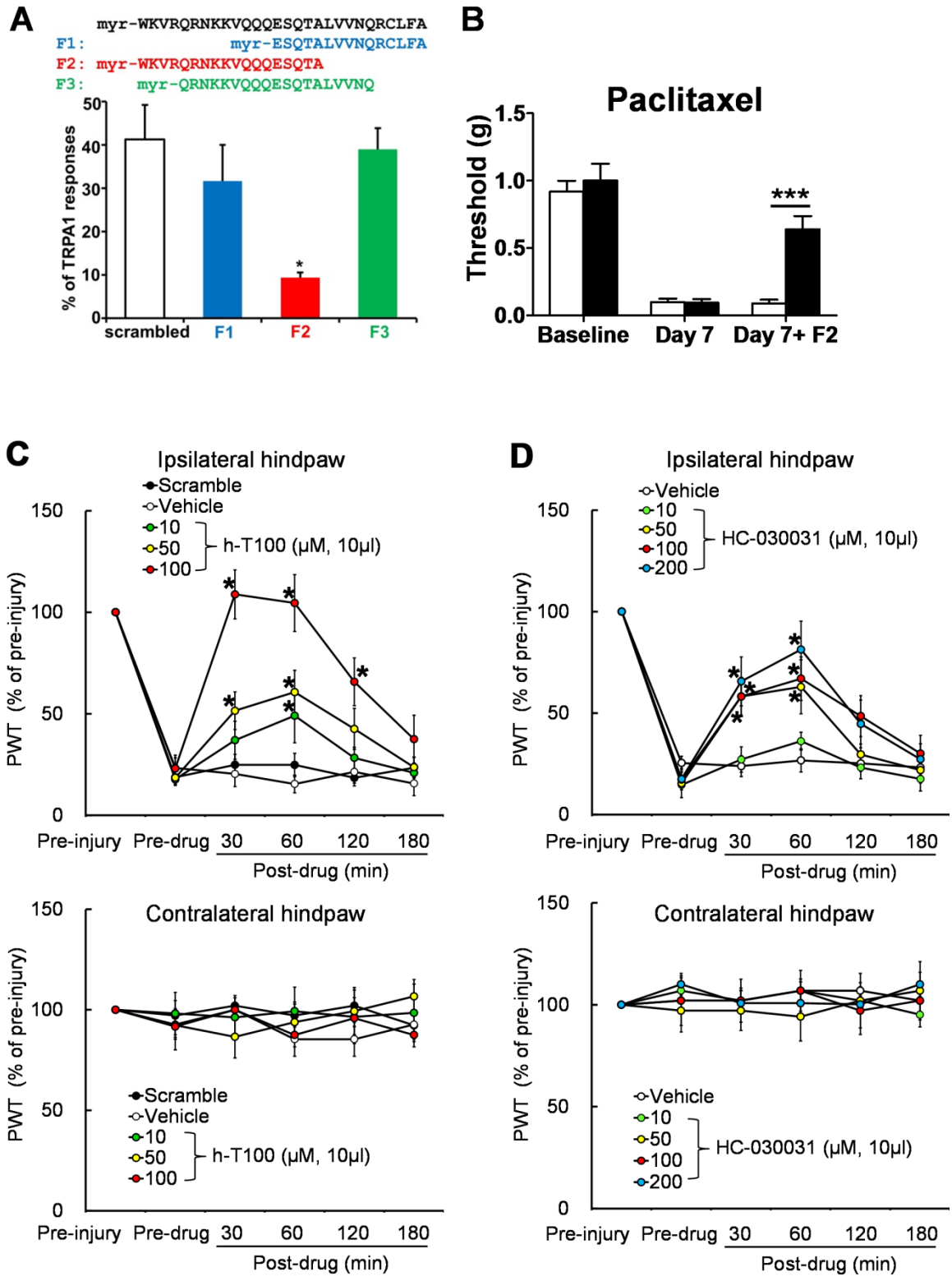

Figure S7. Related Figure 7. A shortened version of cell-permeable peptide (CPP) derived from T100-Mut, F2, is also effective for inhibiting TRPA1 activities in the

heterologous system and painful behavioral models. (**A**) Calcium imaging data from HEK293 cells expressing TRPA1 and TRPV1. Among the three shortened CPP (sequences on top), only F2 (2 μM) significantly reduced the percentage of cells responsive to CA (10 μM) compared to the scrambled (repeated 3 times). The top sequence is from T100-Mut. The scrambled sequence is identical to Figure 7A. *p<0.05. (**B**) F2 (5 μl 100 μM; intradermal injection) is also effective in suppressing paclitaxel-induced mechanical hyperalgesia. n=5, ***p<0.01. Open box: scrambled; black box: F2. Intrathecal injection of human T100-3Q peptide (h-T100) and HC-030031 dose-dependently inhibits neuropathic mechanical hypersensitivity in rats (**C**,**D**). **(C)** In rats with spinal nerve ligation (SNL), intrathecal injection of h-T100 (10–100 μM, 10 μl, n=7-8/dose) dose-dependently increased ipsilateral paw withdrawal thresholds (PWT) from pre-drug levels, reflecting attenuated mechanical hypersensitivity. Intrathecal injections of scrambled peptide (100 μM, 10 μl, n=6) and vehicle (n=5) had no effect. There was no significant change in the contralateral PWT after drug injection. **(D)** Intrathecal injection of HC-030031 (10–200 μM, 10 μl, n=6/dose), a selective TRPA1 receptor antagonist, also increased ipsilateral PWTs of SNL rats in a dose-dependent fashion. Intrathecal injection of vehicle (n=6) was not effective. Contralateral PWTs did not change significantly after drug treatment. T100-Mut peptide has a lower EC_{50} for inhibiting pain (29.3 μM, 10 μl) than HC030031 (58.2 μM, 10 μl). *P<0.05, versus pre-drug. One-way repeated measures ANOVA. All bars are presented as mean ± SEM.

Methods

Molecular biology and biochemistry

Generation of Tmem100 GFP knock-in mouse line: Full-length *Tmem100* cDNA from mouse DRG was cloned into the pGEM T-Easy vector (Promega) and later subcloned into the expression vector pcDNA3.1. The arms of the *Tmem100* targeting constructs were subcloned from ES cell genomic DNA. The gene deletion constructs eliminated exon 3, which contains the entire coding region of *Tmem100*. PmeI and AscI restriction sites were engineered so the EGFPf-ACN cassette could be placed in the middle of the two arms. We also placed a negative selection marker (DTA) outside of the right arm to increase homologous recombination rate. $Tmem100^{GFP/+}$ mice were generated using the targeting construct by the Transgenic Core Laboratory at the Johns Hopkins University. Generation of the mutant allele and excision of the ACN cassette were verified by PCR and Southern blotting.

Generation of *Tmem100* conditional knockout mice: A BAC clone containing the entire *Tmem100* genomic sequence was purchased from Children's Hospital Oakland Research Institute and modified by recombineering (Liu et al., 2003). The final gene targeting vector contains exon 3 and a *PGK-Neo* cassette flanked by two loxP sites. The two homologous arms are 1.9 and 6.0 kb in size, respectively. $Tmem100^{fl/+}$ mice were generated using the targeting construct by the Transgenic Core Laboratory at the Johns Hopkins University. Homologous recombination in ES cells was verified by PCR for both arms with a long range PCR kit (Roche, 04829034001) and sequencing. Germline transmission was confirmed by PCR. The F1 progeny were mated with *FlpE* mice to eliminate the *PGK-Neo* cassette, and the results were verified with PCR targeting the *Neo*

cassette. For the behavioral studies, mice were crossed with WT C57/BL6 for more than 5 generations before mating to an *Avil*$^{+/CRE}$ line.

Western blot of DRG lysate: DRG from cervical to lumbar levels were collected in 300 μL PBS and 2% SDS with protease inhibitor (Sigma P8340). After sonication, the solution was centrifuged at 18,000 rcf for 5 minutes in 4 degrees. The supernatants were collected and stored at -80 degrees. For the western blots, DRG lysates were separated by SDS-PAGE (10% or 15% for Tmem100 detection) and wet transferred to PVDF membranes (GE Healthcare, RPN303F). The membranes were blocked with 5% milk in TBST for 30 minutes. The primary antibodies used were: 1:5000 anti-Tmem100, 1:1000 anti-TRPV1 (Santa Cruz, R130), and 1:1000 anti-TRPA1 (Novus, NB110-40763). Secondary antibodies for visualization included donkey ant-rabbit and anti-mouse HRP-conjugated antibodies (GE Biosciences). The intensities for the signals were analyzed using ImageJ.

Co-immunoprecipitation (Co-IP): DRG from all levels or CHO cells transfected with *Trpv1*, *Trpa1*, and *Tmem100-myc* were used. Whole cell DRG or CHO cells lysates were generated 24 h after transfection, and Co-IP with either 1 μg myc antibody (EMD Millipore) or 1 μg TRPV1 antibody (Santa Cruz, R130) as described (Akopian et al., 2007). Immunoprecipitants and cell lysate aliquots were resolved by SDS-PAGE and immunoblotted with 1:1000 anti-TRPV1 antibody (Santa Cruz, R130), 1:500 anti-Tmem100 antibody, 1:1000 anti-TRPA1 (Novus), or 1:1000 anti-myc (EMD Millipore). Secondary antibodies for visualization included donkey ant-rabbit and anti-mouse HRP-conjugated antibodies (GE Biosciences).

GST pull-down**:** The GST-N, GST-C fusion, and GST constructs (2 μg) were individually transfected with 2 μg of *Trpa1*, *Trpv1*, *Trpm8*, and *Trpv2* constructs into HEK293T cells with Lipofectamine 2000. Twenty-four hours later, cells were washed with PBS and lysed with 500 μL IP buffer (1% Triton X-100 + protease inhibitor in PBS). After sonication and centrifugation for 10 min at 13,000 rpm at 4°C, the supernatants were incubated with glutathione-agarose beads (GE bioscience). The bound proteins were eluted from the beads by heating in 2X protein sample buffer at 50°C for 10 minutes. The samples were resolved by SDS-PAGE and immunoblotted with 1:2500 rabbit polyclonal anti-TRPV1 antibody (Santa Cruz, R130), 1:1000 rabbit anti-TRPA1 antibody (Novus), 1:5000 anti-GST antibody (Sigma A7360), or 1:10000 donkey anti-rabbit HRP-conjugated antibody (GE Bioscience NA934V).

Behavioral assays

Hot plate methods: Mice were placed in a clear plexiglass cylinder on top of a temperature-controlled metal plate (Life Science Series 8, Model 39.) The latency of acute nocifensive responses was determined by the onset of hindpaw lifts and/or licking, flinching, or jumping.

Tail immersion test: Mice were restrained in an apparatus made of 50 mL conical tubes. Their tails were exposed in the water bath set to the designated temperatures.

Von Frey methods: Mice were placed in a transparent plastic box (4.5 × 5 × 10 cm) on a metal mesh and acclimatized for 30 minutes prior to testing. Each mouse was tested more than 5 times at a specific force manually, and the threshold was determined by the lowest force needed to elicit responses more than 50% of the time.

Mustard oil injection: Mice were injected intradermally in the hind paw with 6μL of 0.2% mustard oil (Sigma-Aldrich 377430) with Hamilton needles (80300). The mice were placed in a plexiglass cylinder, and the total time spent licking and flinching was recorded for the first 10 minutes after injection. Thirty and sixty minutes after injection, the mice were assayed with von Frey filaments for mechanical hyperalgesia.

Hargreaves test: Mice were placed under a transparent plastic box (4.5 × 5 × 10 cm) on a glass platform (Plantar Test Apparatus, IITC Life Science). Radiant heat was adjusted to 18% of maximal output and shone on the center of the paws. Each mouse was tested more than 3 times, with each test performed 20 minutes apart.

CFA injection: Mice were injected with 6 μL of 50% emulsified *Complete Freund's Adjuvant (Sigma, F5881) in normal saline.*

Capsaicin injection: Mice were injected with 6 μL of capsaicin (0.1 μg/μL in normal saline/10% ethanol/ 0.5% Tween 80) in the hindpaws. The mice were placed in a plexiglass cylinder, and the total time spent licking and flinching was recorded for the first 10 minutes after injection.

Paclitaxel injection: Mice were injected with paclitaxel (Sigma T7191) intraperitoneally at the dose of 6mg/kg, as previously described (Materazzi et al., 2012). Seven days after paclitaxel injection, the mice were assayed with Von Frey methods for mechanical hyperalgesia, both before and four hours after injection of cell permeable peptides.

Cold plate test: a metallic plate on a bed of ice was cooled in a −20 °C freezer. During the test, the plate was allowed to warm to 0 °C as measured by the temperature probe. The onset of brisk hindpaw lifts and/or flicking/licking of the hindpaw was assessed.

Rat L5 SNL: An modified L5 SNL model was produced as described in our previous studies (He et al., 2014;Shechter et al., 2013). Male Sprague-Dawley rats (200–350 g, Harlan, Indianapolis, IN) were anesthetized with 2% isoflurane. The left L5 spinal nerve was ligated with a 6-0 silk suture and cut distally. The muscle layer was closed with 4-0 chromic gut suture and the skin closed with metal clips. For intrathecal catheter implantation, a small slit was cut in the atlanto-occipital membrane of rats, into which a saline-filled piece of PE-10 tubing (6–7 cm) was inserted (He et al., 2014). After completing the experiment, we confirmed intrathecal drug delivery by injecting lidocaine (400 μg/20 μl, Hospira, Lake Forest, IL), which resulted in a temporary motor paralysis of the lower limbs. Hypersensitivity to punctuate mechanical stimulation was determined with the up-down method by using a series of von Frey filaments (0.38–15.1 g) applied for 4–6 seconds to the test area on the plantar surface of the hindpaw (Chaplan et al., 1994; He et al., 2014). The PWT was determined according to the formula provided by Dixon (Dixon, 1980). Rats that underwent SNL but did not develop mechanical hypersensitivity (>50% reduction of PWT from pre-SNL baseline) by day 5 post-SNL and rats that showed impaired motor function or deteriorating health after treatment were eliminated from the subsequent behavioral studies, and data were not analyzed. HC-030031 was purchased from Tocris Bioscience (Bristol, UK). Both drugs were dissolved in 10% dimethylsulfoxide (DMSO), 5% Tween 80 and 85% sterile saline solution. The final working solution which was injected by intrathecal route contained <1 % DMSO. The number of animals used in each study was based on our experience with similar studies and power analysis calculations. We randomized animals to the different treatment groups and blinded the experimenter to drug treatment to reduce selection and

observation bias. After the experiments were completed, no data point was excluded. STATISTICA 6.0 software (StatSoft, Inc., Tulsa, OK) was used to conduct all statistical analyses. The Tukey honestly significant difference (HSD) post-hoc test was used to compare specific data points. Bonferroni correction was applied for multiple comparisons. Two-tailed tests were performed, and data are expressed as mean ± SEM; $P<0.05$ was considered significant in all tests.

Calcium imaging

Calcium imaging assays were performed as previously described (Liu et al., 2009). Cells were loaded with 2 μM fura 2-acetomethoxy ester (Molecular Probes) for 30 min in the dark at room temperature or for 45 minutes at 37°C for DRG and cell lines, respectively. After washing, cells were imaged at 340 and 380 nm excitation to detect intracellular free calcium under a fluorescent microscope (Nikon Eclipse TE2000-S) and Lambda 10B shutter (Sutter Instrument). The cells were bathed in calcium imaging buffer (pH 7.45, 130mM NaCl, 3mM KCl, 2.5mM $CaCl_2$, 10mM HEPES, 10mM glucose, 1.2mM $NaHCO_3$, with sucrose to increase osmolarity to 290mOsm). The reagents and buffers were applied through a gravity perfusion system at a rate of 2mL/s, including mustard oil (Sigma 377430), cinnamaldehyde (Sigma C80687), menthol (Sigma M2780), and capsaicin (Sigma M2028). Cells with high baseline 340/380 values (>1.5) were excluded for analysis. For DRG neurons, IB_4 staining was performed in the chamber with the dilution of 1:200 (Molecular Probes I21412) for 160 seconds before washing off at the end of each test. Images were processed and analyzed with NIS-Elements BR 2.30 software (Nikon). A responsive cell was defined as one that with greater than a 20% increase in the 340/380 ratio above the baseline. Intracellular calibration for calcium was

performed as previously described (Akopian et al., 2007). The data was analyzed with the experimenter blinded to the genotypes or constructs transfected.

Cell culture

DRG from 3 to 4-week old mice were collected in cold DH10 medium (90% DMEM/F-12, 10% FBS, 100 U/ml penicillin, and 100 μg/ml Streptomycin, Gibco) and treated with enzyme solution in HBSS containing collagenase (1.65mg/mL, Worthington CLS I) and dispase (3.55mg/mL, GIBCO 17105-041) at 37 °C for 30 minutes. After trituration and centrifugation, cells were resuspended in DH10, plated on glass coverslips coated with poly-D-lysine (0.5 mg/ml, Stoughton, MA) and laminin (10 μg/ml, Invitrogen), and cultured overnight in an incubator at 37°C. The neurons were tested within 24 hours. HEK293T, COS-7, and CHO cells were cultured in a medium consisting of 90% DMEM, 10% FBS, 100 U/mL penicillin, and 100 μg/ml Streptomycin. GlutaMAX (Gibco 35050-061) was also added for CHO cells. For calcium imaging, the cells were plated on glass coverslips coated with poly-D-lysine (0.5 mg/ml, Stoughton, MA). In the HEK cell studies our denominator is the cells expressing both TRPA1, TRPV1, and the designated constructs (i.e. Tmem100 or Tmem100-3Q mutant). We transfected mCherry:TRPV1:Tmem100 in 1:8:8 ratio into TRPA1 stable cell line (obtained from N. Tigue from GlaxoSmithKline) and used mCherry as the marker for the cells expressing the constructs 18 hours after transfection with Lipofectamine 2000. The transfection efficiency for Tmem100+TRPV1+TRPA1 triple-positive cells is 27 ± 3%. This efficiency was determined by mCherry(+) divided by total number of cells in the bright fields.

Electrophysiology

Recordings were made in cell-attached single-channel or whole-cell voltage clamp configurations at 22-24^{o}C from the somata of small-to-medium mouse DRG neurons (15-35 pF) or CHO cells. For whole-cell configuration, holding potential (Vh) is –60mV. Data were acquired and analyzed using an Axopatch 200B amplifier and pCLAMP9.0 software (Molecular Devices, Sunnyvale, CA). Borosilicate pipettes (Sutter, Novato, CA) were pulled and polished to resistances of 3-5 MΩ (in whole-cell and single-channel pipette solutions). Access resistance (Rs) was compensated (40-80%) when appropriate up to the value 7-10 MΩ for whole-cell configuration. Whole-cell recording data were filtered at 0.5 kHz and sampled at 2 kHz. Single-channels currents were filtered with an 8-pole, low pass Bessel filter at 0.1 kHz and sampled at 0.5 kHz, since dwelling time (τ) of the TRPA1 and TRPV1 single-currents were >0.5 sec. Whole-cell recorded data were rejected when Rs changed >20% during recording, leak currents were >100pA, or input resistance was < 200 MΩ. Currents were considered positive when their amplitudes were 5-fold bigger than displayed noise (in root mean square).

Single-channel unitary current (i) was determined from the best-fit Gaussian distribution of amplitude histograms. Single-channel activity was analyzed as NPo = I/i, where I is the mean total current in a patch and i is unitary current at this voltage. Open probability (Po) for main conductance is presented in figures. For single channel slope conductances, linear fitting was used separately for positive and negative holding potentials. The slope conductances presented in figures were determined from fitting negative hold potentials (from -60 to 0 mV). The single-channel recording data were analyzed with Clampfit 9 software. This has an “event detection analysis” function that analyzes current traces and determines the number of channels in the patch (N), how

many sub-conductances are present, and what the main conductance is. In order to increase the accuracy of the Po measurement, only patches containing fewer than 3 channels were used. For patches containing both TRPA1 and TRPV1, only those with equal numbers of TRPA1 and TRPV1 were used. This was monitored in each recording by applying MO and then CAP.

Standard external solution (SES) for whole-cell patch recording contained (in mM): 140 NaCl, 5 KCl, 2 $CaCl_2$, 1 $MgCl_2$, 10 D-glucose and 10 HEPES, pH 7.4. Vehicle, which is 0.01% DMSO, was added to external solutions. The bath solution for single-channel recording (SES-SCh) of TRP currents consisted of (in mM): 100 K-gluconate, 4 KCl, 1 $MgCl_2$, 1 EGTA, 10 D-glucose and 10 Hepes (pH 7.3). The standard pipette solution (SIS) for the whole-cell configurations contained (in mM): 140 KCl, 1 $MgCl_2$, 1 $CaCl_2$, 10 EGTA, 10 D-glucose, 10 HEPES, pH 7.3. The pipette solution for single-channel recording (SIS-SCh) was (mM): 100 Na-gluconate, 10 NaCl, 1 $MgCl_2$, 2 $CaCl_2$, 10 D-glucose and 10 HEPES (pH 7.3). Drugs were applied using a fast, pressure-driven, computer controlled 8-channel system (ValveLink8; AutoMate Scientific, San Francisco, CA). The baseline activities of the cells were recorded for 1-2 min prior drug applications. The durations of drug applications are noted in legends to figures. Single-channel analyses of traces were performed from the 10th to 30th seconds after commencing drug applications.

Immunofluorescent staining

Adult mice of 8-12 weeks old were anesthetized with pentobarbital and perfused with 20 ml 0.1 M phosphate-buffered saline (PBS; pH 7.4; 4 degrees) followed with 25 ml 4% paraformaldehyde and 14% picric acid in PBS (4 degrees). After perfusion, spinal

cords and dorsal root ganglia (DRG) were dissected. DRG was post-fixed in 4% paraformaldehyde and 14% picric acid at 4 degrees for 30 min and spinal cord was fixed for 1 hr. All tissues were cryoprotected in 20% sucrose in PBS at 4 degrees overnight, and preserved in OCT at – 80 degree. Before staining, twenty μm sections were post-fixed with 4% paraformaldehyde in PBS for 10 minutes and washed with 0.1% PBST. After blocking in 10% goat serum in PBST for 1 hour at room temperature, sections were incubated with primary antibodies at 4°C overnight. The primary antibodies used were: rabbit anti-GFP (Invitrogen, 1:1000), chicken anti-GFP (Invitrogen, 1:1000), rabbit anti-CGRP (Bachem T-4239, 1:1000), rabbit anti-NF200 (Sigma N4142, 1:1000), rabbit anti-TRPV1 (gift from Dr. Caterina, 1:1000), IB_4 (Molecular Probes I-21412, 1:200), mouse anti-NeuN (Millipore MAB377, 1:300), and rabbit anti-TRPA1 (gift from Dr. Schmidt, 1:200). On the second day, the sections were incubated with secondary antibodies at room temperature for 1 hour. The secondary antibodies used were: goat anti-rabbit (Invitrogen A11036, Alexa 568-conjugated; A11034, Alexa 488-conjugated), goat anti-chicken (Invitrogen A11039, Alexa 488-conjugated), goat anti-rat (Invitrogen A11434, Alexa 555-conjugated), and goat anti-mouse IgG1 (Invitrogen A-21124, Alexa 568-conjugated; A-21121, Alexa 488 conjugated). All secondary antibodies were diluted 1:300 in the blocking solution. Sections were washed with PBST and mounted with Fluoromount-G (Southern BioTech). Images were obtained using the Zeiss LSM700 confocal microscope system.

Live staining

F11 cell line was transfected with 0.6 μg of either $pcDNA_{3.1}$-Tmem100-myc or $pcDNA_{3.1}$-Tmem100 +0.2μg mCherry following Lipofectamine 2000 protocol. On the

second day, the cells were trypsinized and plated on 150 mm coverslips coated with poly-D-lysine. The non-detergent-treated (NDT) groups were washed 3 times with buffer consisting of 1% goat serum in PBS. The detergent-treated (DT) groups were fixed with 4% PFA in PBS for 15 minutes at room temperature and washed with buffer consisting of 1% goat serum in 0.1% PBST. After washing, the coverslips were blocked in 10% goat serum in their respective washing buffers for 15 minutes at room temperature. They were incubated with primary antibodies (1:200 mouse anti-c-myc ab, 9B11, 1mg/mL) or 1:1000 rabbit anti-Tmem100 antibody for 1 hour at room temperature and washed 3 times. They were incubated with secondary antibodies (1:1000 goat anti-mouse IgG-488 (Invitrogen) or goat anti-rabbit IgG-488 (Invitrogen)) for 30 min at room temperature.

Total internal reflection fluorescence (TIRF) microscopy and Förster resonance energy transfer (FRET)

Expression vectors of pEYFP-TRPA1 (YFP on C-terminal part), pECFP-TRPV1 (CFP on C-terminal part), and pEYFP-N1 were transfected into COS-7 cells with FuGENE HD (Promega E2311), as previously described (Staruschenko et al., 2010). COS-7 cells were chosen since they have flat morphology and thus suitable for TIRF-FRET analysis. Moreover, previously it has been shown that CHO and COS cells express TRPA1 and TRPV1 to the same level(Staruschenko et al., 2010). Data from fixed cells were collected in separate facilities at University of Texas Health Science Center, San Antonio, and the Johns Hopkins University, respectively. Each group was co-transfected with full-length pcDNA$_{3.1}$-Tmem100, pcDNA$_{3.1}$-Tmem100-3Q, or pcDNA$_{3.1}$-myc/His and plated on glass-bottom dishes (MatTek, P35G-1.0-14-C). FRET was essentially performed as previously described (Staruschenko et al., 2010). Briefly, two days after

transfection, the cells were fixed for 15 min with 4% paraformaldehyde in PBS and then imaged at the room temperature using total internal reflection fluorescence (TIRF) (also called evanescent-field) microscopy on an inverted Nikon Eclipse TE200U microscope equipped with a plain Apo TIRF 60x oil-immersion, high-resolution (1.45 NA) objective. The CFP and YFP fluorophores were excited with a 442-nm Melles Griot dual-pulsed solid state and 514-nm argon ion laser, respectively, with an acoustic optic tunable filter used to select excitation wavelengths (Prairie Technology, Middleton, WI). Emissions from CFP and YFP passed through an image splitting device (Dual-View, Optical Insights, Tucson, AZ) using a 505-nm dichroic filter to split emissions, which then passed through 470 ± 15 and 550 ± 25 nm emission filters, respectively. Fluorescence images were collected and processed with a 16-bit, cooled charge-coupled device camera (Cascade 512F; Roper Scientific Inc.) interfaced to a PC running Metamorph software.

Each cell was photobleached by argon-ion laser (514 nm) at full power for 2 min. We have demonstrated previously preferential photo-bleaching of membrane proteins in and near the plasma membrane abutting the coverglass *versus* total cellular pools of the channel with TIRF illumination (Staruschenko et al., 2010). The %FRET efficiency was calculated as the percent increase in CFP after photobleaching:

$$\%FRET = (CFPpost - CFPpre) / CFPpost$$

where CFPpost and CFPpre are the mean grey values of CFP emission in the cells after and before photobleaching subtracted by its background, respectively. All images were analyzed in ImageJ.

Cell permeable peptides

The sequence from the last 28 amino acids of the C-terminus of the Tmem100-3Q mutant protein was synthesized and myristoylated at its N-terminus (myr-WKVRQRNKKVQQQESQTALVVNQRCLFA-COOH) by Twentyfirst Century Biochemicals. The scrambled peptide was synthesized with the same composition and did not resemble any known protein (myr-QRVLEQVLQNWSRRANVKQAQKFQVKCT – COOH). For the calcium imaging assay, the peptides were added to the calcium imaging buffer with a final concentration of 200 nM and incubated for at least 30 min at room temperature. For the mice behavioral assays, the peptides (5 μL, 2 mM) were injected subcutaneously in the hindpaw at least 30 minutes before testing. For the rat behavior assays, human T100-3Q (h-T100), a palmitoylated cell permeable peptide mutated based on the C terminus of human sequence in Tmem100, was applied. The sequence is Palmitoyl-WKVRQRSKKAQQQESQTALVANQRSLFA-COOH.

References

Akopian, A.N., Ruparel, N.B., Jeske, N.A., and Hargreaves, K.M. (2007). Transient receptor potential TRPA1 channel desensitization in sensory neurons is agonist dependent and regulated by TRPV1-directed internalization. The Journal of physiology 583, 175-193.

Chaplan, S.R., Bach, F.W., Pogrel, J.W., Chung, J.M., and Yaksh, T.L. (1994). Quantitative assessment of tactile allodynia in the rat paw. J Neurosci Methods 53, 55-63.

Dixon, W.J. (1980). Efficient analysis of experimental observations. Annu Rev Pharmacol Toxicol 20, 441-462.

He, S.Q., Li, Z., Chu, Y.X., Han, L., Xu, Q., Li, M., Yang, F., Liu, Q., Tang, Z., Wang, Y.*, et al.* (2014). MrgC agonism at central terminals of primary sensory neurons inhibits neuropathic pain. Pain 155, 534-544.

Liu, P., Jenkins, N.A., and Copeland, N.G. (2003). A highly efficient recombineering-based method for generating conditional knockout mutations. Genome research 13, 476-484.

Liu, Q., Tang, Z., Surdenikova, L., Kim, S., Patel, K.N., Kim, A., Ru, F., Guan, Y., Weng, H.J., Geng, Y.*, et al.* (2009). Sensory neuron-specific GPCR Mrgprs are itch receptors mediating chloroquine-induced pruritus. Cell 139, 1353-1365.

Materazzi, S., Fusi, C., Benemei, S., Pedretti, P., Patacchini, R., Nilius, B., Prenen, J., Creminon, C., Geppetti, P., and Nassini, R. (2012). TRPA1 and TRPV4 mediate paclitaxel-induced peripheral neuropathy in mice via a glutathione-sensitive mechanism. Pflügers Archiv-European Journal of Physiology 463, 561-569.

Staruschenko, A., Jeske, N.A., and Akopian, A.N. (2010). Contribution of TRPV1-TRPA1 interaction to the single channel properties of the TRPA1 channel. The Journal of biological chemistry 285, 15167-15177.